Mechanical Systems and Signal Processing 227 (2025) 112399

Contents lists available at ScienceDirect

Mechanical Systems and Signal Processing

journal homepage: www.elsevier.com/locate/ymssp

Investigation on impact behavior with viscous damping and tensile force inspired by Kelvin-Voigt model in granular system

Gengxiang Wang [a,b,*], Matthias G.R. Faes [c], Tengfei Shi [d], Fuan Cheng [a,*], Yongjun Pan [e]

[a] School of Mechanical and Electrical Engineering, Xi'an University of Architecture and Technology, Xi'an 710055, Shaanxi, China
[b] Institute for Interdisciplinary and Innovate Research, Xi'an University of Architecture and Technology, Xi'an 710064, China
[c] Chair for Reliability Engineering, TU Dortmund University, Dortmund, Germany
[d] Applied Mechanics and Structure Safety Key Laboratory of Sichuan Province, School of Mechanics and Aerospace Engineering, Southwest Jiaotong University, Chengdu 610031, China
[e] College of Mechanical and Vehicle Engineering, Chongqing University, Chongqing 400044, China

ARTICLE INFO

Keywords:
Kelvin-Voigt model
Solitary wave
Loss factor
Viscous damping
Granular system

ABSTRACT

This investigation proposes a continuous contact model with different viscous damping factors by employing the physical properties of the Kelvin-Voigt model. The viscous damping coefficient is treated as a function of the loss factor and frequency. The loss factor in the elastoplastic or plastic phase is obtained by solving the linear equation of motion, because the elastoplastic contact stiffness can be assumed to be approximately linear. The loss factor in the elastic phase is derived according to the energy conservation during impact. Two loss factors in the frequency-dependent damping coefficients govern the energy dissipation in the entire contact behavior. More importantly, the proposed contact model inherits the deficiency of the Kelvin-Voigt model, which exhibits a tensile force at the end of the recovery phase. The underlying reason for this phenomenon is revealed. Simultaneously, it is also explained why the tensile force does not affect the solitary wave propagation in the granular system. Performed simulations show that the proposed contact model not only sidesteps the numerical issues corresponding to most contact force models with hysteresis damping factors, but also compensates for the accuracy loss of the EDEM contact model when evaluating the elastoplastic contact behavior in the granular system.

1. Introduction

One-dimensional granular chains serve as the most straightforward granular system [1]. However, they also possess a list of unpredictable behavior types, including highly nonlinear, strongly localized solitary waves [2]. This feature leads to potential applications [3], such as shock absorbers [4], impulse protectors[5], impact mitigation [6], vibration filter [7], and so on. However, before these systems can be successfully applied, the intrinsic dynamic properties between the particles should be understood [8,9]. Actually, the propagation features of the solitary waves [10] in the granular chain are closely related to the contact force between the particles [11]. Therefore, an accurate contact force model plays a crucial role in calculating the contact force between the particles. Currently, there are two kinds of contact force models applied in granular system theory: (i) the static elastoplastic contact models [12]; (ii) the

* Corresponding authors.
E-mail addresses: wanggengxiang@xauat.edu.cn (G. Wang), chengfuan@xauat.edu.cn (F. Cheng).

https://doi.org/10.1016/j.ymssp.2025.112399
Received 5 June 2023; Received in revised form 21 October 2024; Accepted 23 January 2025
Available online 30 January 2025

Nomenclature

A	Amplitude
c_r	Coefficient of restitution
D_1	Frequency-dependent damping coefficient
D_2	Nonlinear elastic damping coefficient
E_i	Young's modulus of contact body i
F	Contact force
F_{np}	Contact force in the elastoplastic or plastic phase
F_e	Contact force in the elastic phase
F_{dem}	Contact force calculated based on the contact model used in EDEM software
g_1	loss factor in the elastoplastic phase
g_2	loss factor in the elastic phase
K	Stiffness coefficient of spring
K_h	Hertz contact stiffness coefficient
K_p	Linearized contact stiffness coefficient
M	Mass of the contact body
p_y	Critical value of yielding
R_i	Radius of contact body i
R^e_{ep}	Curvature Radius in the elastoplastic phase
R^e_p	Curvature Radius in the plastic phase
t	Time
ΔE	Dissipated energy
ν_i	Poisson ratio of the contact material of the contact body i
δ	Relative deformation between contact bodies
δ_p	Critical plastic deformation
δ_y	Critical elastic deformation
$\delta_{\max}$	Maximum contact deformation
$\dot{\delta}^{(-)}$	Initial impact velocity
$\dot{\delta}$	Impact velocity
$\dot{\delta}_f$	Post-impact velocity
σ_y	Yield stress
ε	Dimensionless geometric parameter for uniform contact
ψ	Ratio between Brinell hardness and yielding strength
ω	Natural Frequency
ω_d	Frequency
ξ	Damping
ϕ	Phase angle

continuous contact force model extended based on Hertz's contact law [13].

As for the static elastoplastic contact models [12], their constitutive relations are developed by a quasi-static pressure test ignoring the strain rate variation or plastic flow [14]. The contact process is generally divided into three phases: elastic, elastoplastic, and full plastic [15]. In the elastic phase, Hertz's contact law provides a closed mechanics constitutive relation [16]. Once the contact deformation exceeds the critical elastic deformation, the contact behavior is governed by the Mises yield theory, rather than Hertz's contact law [17]. The analytical solution of the constitutive relation can be derived based on the Mises yield theory when the contact comes into the full plastic phase [18]. In this stage, some scholars have developed a series of constitutive relations in the full plastic phase, such as Brinell [19], Tabor and Ishlinskii [20], Lee et al.[21], and Follansbee and Sinclair[22], and so on. However, in the real static compression test, the contact process between the elastic phase and full plastic phase exists a transition phase that is the elastoplastic phase [23,24]. The discontinuity is subject to be generated if the elastoplastic phase is ignored. Thereby, a rational constitutive relation of the elastoplastic phase can make the contact behavior transit from the elastic phase to the full plastic phase smoothly. Nevertheless, it is hard to obtain an analytical solution for the elastoplastic phase by directly solving the mechanics equations [25], such as the CEB model developed by Chang, Etsion and Bogy [26], and the ZMC model proposed by Zhao, Maletta and Chang. To achieve the continuous constitutive equations of the static elastoplastic contact behavior, most scholars resorted to the Finite Element Method (FEM) and fit the constitutive curve using a polynomial interpolation scheme. Such an approach was followed by, e.g., Johnson [27], Stronge [28], Jackson and Green [29], Kogut and Etsion [30], Shankar and Mayuram [31], Zhang and Vu-Quoc [32,33], Du and Wang [34], Brake [12], Komvopoulos and Ye [35]. In particular, Burgoyne and Daraio proposed a quasi-static elastoplastic contact model used to describe solitary wave propagation in the one-dimensional granular chain by FEM [36,37]. In addition to this, Ma and Liu (ML model) utilized reasonable boundary conditions to improve the constitutive relation in the elastoplastic contact phase

to fix the discontinuous transition between the elastic and full plastic phases and developed a piecewise and continuous contact model based on the Johnsons' elastoplastic contact theory [38]. On this basis, Feng et al. employed this static contact model to reproduce the solitary wave propagation obtained by Burgoyne and Daraio [39], which manifested the effectiveness of the Ma-Liu model. However, since the static elastoplastic contact models adopted the different constitutive equations between the loading and unloading path, the compression and recovery phase must be recognized in each impact [36,40,41]. Furthermore, the maximum and residual contact deformations need to be calculated and saved, as well as prepared for the ensuing contact event in the granular chain [36,39,41–43]. The computational strategy related to predicting the elastoplastic contact behavior in the granular chain is very complicated, and even fails to simulate this behavior when facing a huge number of particles [44]. That is why the static elastoplastic contact models are not widely used in the EDEM software [45].

Continuous contact force models that consider the energy dissipation have a concise mathematical form [13,46]; more importantly, unlike the static elastoplastic contact models, they employ a damping loop to represent the energy dissipation [47], rather than using the discrepancy between the loading and unloading path. This is a benefit for the calculation of the contact behavior in the multibody system [48]. As such, this topic recently attracted a lot of research attention [13,46,49–52]. Recently, there have been several review papers discussing the development history [53]. Hertz serves as the pioneer in developing the contact mechanics between two perfectly elastic bodies; however, it cannot describe the energy dissipation during contact. Kelvin and Voigt adopted the linear spring-damper model to develop the contact model and used the damping term to represent energy dissipation [48]. Nevertheless, the damping term with a constant damping coefficient leads to discontinuity at the beginning of the compression and the end of the recovery phase [54,55]. Subsequently, Hunt and Crossley eliminated this deficiency by assuming that the damping coefficient is a function of the contact deformation [56]. After that, to describe energy dissipation more accurately, a series of hysteresis damping coefficients were developed by considering several approximative methods [57–64]. The derivation process of these hysteresis damping factors [65] is essentially based on energy and momentum conservation during contact. Therefore, hysteresis damping is also referred to as frequency-independent damping [65]. These continuous contact force models have been successfully applied to calculate contact behavior in the multibody system [48,66]. However, it is worth noting that the contact models with frequency-independent damping cannot be used to evaluate the impact event when the relative impact velocity is very small or equal to zero [67]. Because the denominator of the hysteresis damping factor, including the initial impact velocity, leads to the numerical singular issues [51,52,68–70]. That is why the EDEM software does not use the continuous contact force model with a hysteresis damping factor.

In order to bypass this problem, some scholars developed the viscous damping coefficient, which is also called "frequency-dependent damping". Hereto, they solve the single nonlinear degree of freedom vibration equation [70–72], such as, e.g., Kuwabara and Kono [73], Tsuji et al.[45], Jankowski [74,75], Lee and Wang [58]. In addition to these developments, some scholars directly employed the empirical value to represent the damping coefficient to sidestep the numerical singular issues caused by the denominator of the damping factor [57,76], such as Schwager and Poschel [76], Lee and Herrmann [57], and Ristow [77]. At this point, Tsuji et al. [45] derived a viscous damping factor based on the Hertz contact law by solving the nonlinear equation of motion using the numerical method. This model has been applied to the EDEM software. However, it is only valid and accurate when a purely elastic contact event happens in the granular system [78,79]. Once the contact phase comes into the elastoplastic phase, the Hertz contact stiffness overestimates the contact stiffness [60,62]. This phenomenon leads to the fact that the contact force obtained using the EDEM contact model is larger than the realistic contact force in the elastoplastic phase. This, in its turn, affects the propagation speed and peak values of the solitary waves in the granular chain. Therefore, a complete contact process should embrace the elastic, elastoplastic, and full plastic phases [37,38]. The viscous damping coefficients in the different contact phases should correspondingly solve the linear or nonlinear equation of motion [50]. Namely, the entire contact process should not be governed purely by the nonlinear or linear vibration system [61]. It should combine the nonlinear characteristic in the elastic phase and linear futures in the elastoplastic or plastic phase [74,75]. Moreover, there are seldom investigations to focus on the tensile force area [80] in the viscous damping loop obtained from the contact models with frequency-dependent damping [81]; even there are no references [82] to study the effect of the tensile force area on the solitary wave propagation in the granular system. It is the primary motivation for the investigation.

1.1. Limitations and main contributions

At present, the contact force models applied to simulate the solitary wave propagation present certain limitations in the granular chain as follows:

(1) As for the continuous contact force model with a hysteresis damping factor, there are at least two restrictions: (i) the denominator of the hysteresis damping factor includes the initial impact velocity [13], which is prone to generate numerical singular issues since most particles in the granular system are initially at rest; (ii) they are extended based on the Hertz contact law, which cannot be used to precisely evaluate the elastoplastic contact behavior, as described above.
(2) As for the static elastoplastic contact model, these models can precisely calculate the elastoplastic contact event in the granular chain under high impact velocity [38]. However, its calculation process is extremely sophisticated, and in some cases, it is even impossible to handle the enormous amounts of particles because the compression and recovery phases need to be identified in every single contact [83]. Simultaneously, the maximum and residual contact deformations are also estimated and saved in preparation for the next contact [37]. These reasons explain why the static elastoplastic contact models are not widely used in EDEM software.
(3) As for the contact model applied in EDEM software, although it avoids the numerical singular issues caused by the denominator of the damping factor, the Hertz contact stiffness still overestimates the contact stiffness when the contact behavior comes into

the elastoplastic phase[36,40]. Our group has proved this conclusion in recent work [50]. This phenomenon leads to the approach losing accuracy in simulating the elastoplastic contact event in the granular system.

In light of the above limitations regarding the contact model applied to the granular system, this investigation aims to develop a new contact force model to remove these restrictions from existing contact force models, which is inspired by the Kelvin-Voigt contact model. The current work is completely different from our recent publications [84–86]. Its primary contributions can be summarized as follows:

(1) Since the relationship between the contact force and displacement is approximately linear when the elastoplastic deformation is activated [12], the original idea of the new contact force model is motivated by the Kelvin-Voigt contact model. A linear vibration system with a frequency-dependent damping factor represents the contact process in the elastoplastic or plastic phase [65]. In this system, the contact stiffness is derived from the ML model; the viscous damping factor consists of the loss factor and the frequency of the system [74]. The loss factor in the elastoplastic phase can be obtained by solving this linear vibration system [75]. However, at the beginning of the contact behavior, the elastic phase must be experienced prior to the elastoplastic phase [87]. The assumption of the linear vibration system cannot be applied in the elastic phase. Based on the assumption of the damping factor in the elastoplastic, the frequency-dependent damping factor [65] in the elastic phase is redefined by a new loss factor referred to in literature [74,75]. Therefore, the new contact force model with the viscous damping factor follows the nonlinear Hertz contact law in the elastic phase and complies with the constitutive relation when the contact comes into the elastoplastic phase. It stays completely consistent with the actual elastoplastic contact process.
(2) Since the new contact force model combines the nonlinear properties in the elastic phase and linear features in the elastoplastic phase in the entire contact process, it exhibits the advantages of high precision compared to the contact model applied in the EDEM software [88–90], especially in the elastoplastic or plastic deformation regimes. In addition to this, the tensile force [91] is prone to be activated when the contact process approaches the end of the recovery phase because the post-impact velocity closes to the maximum contact velocity; this reason leads to that the damping force in this phase is larger than the first term in the new contact force model. However, the new contact force model avoids the deficiency of the Kelvin-Voigt model [48]. It is mainly because the new contact force model includes the elastic contact phase, and the viscous damping coefficient includes the contact deformation. Therefore, the entire contact process starts from the zero point and ends at zero. More importantly, this investigation is the first time to reveal why the tensile force has no effect on the contact process between the particles in the granular system. The primary reason lies in the multiple compression and multiple impacts between the particles that prevent the contact force from coming into the tensile force area when the contact behavior approaches the end of the recovery phase.

1.2. Structure of this investigation

The structure of this investigation includes as follows: In Section 2, the ML model is introduced simply. A new contact model with tensile force is proposed in Section 3; moreover, the impact between two spheres is treated as the numerical example to analyze the dynamic performances of the new contact model; simultaneously, the comparison analysis between the new contact model, the EDEM contact model, and Hunt-Crossley is implemented. The vertical and horizontal granular chains and Hopkinson pressure bar are simulated based on the new dashpot model in Section 4. The main conclusions are summarized in Section 5.

2. ML static contact force model

The loading phase of the elastoplastic contact model is described as

$$F(\delta)=\begin{cases}\dfrac{4}{3}ER^{\frac{1}{2}}\delta^{\frac{3}{2}} & \delta<\delta_y\\ \delta\left(c_1+c_2\ln\dfrac{\delta}{\delta_y}\right)+c_3 & \delta_y\le\delta<\delta_p\\ F_p+k_1\left(\delta-\delta_p\right) & \delta\ge\delta_p\end{cases}\tag{1}$$

where $1/E=\left(1-\nu_1^2\right)/E_1+\left(1-\nu_2^2\right)/E_2$, $R=R_1R_2/(R_1\pm R_2)$, $\delta_y=\pi^2Rp_y^2/4E^2$ is the critical elastic deformation, E_1 and E_2 are the Young's modulus of the contact bodies, ν_1 and ν_2 are the Possion ration of the contact bodies, $p_y=1.61\sigma_y$ is the critical value of yielding, σ_y is the yield stress. The parameter $\delta_p=\varepsilon^2\delta_y/2$ is the critical plastic deformation; the physical meaning ε can be spotted in this reference [38]. The coefficient in this contact model is given by

$$\begin{cases}k_1=2\pi R\psi\sigma_y, F_p=\delta_p\left(c_1+c_2\ln\left(\varepsilon^2/2\right)\right)+c_3\\ c_1=\dfrac{p_y(1+\ln(\varepsilon^2/2))-2\psi\sigma_y}{\ln(\varepsilon^2/2)}\pi R, c_2=\dfrac{2\psi\sigma_y-p_y}{\ln(\varepsilon^2/2)}\pi R, c_3=F_y-c_1\delta_y, F_y=\pi^3R^2p_y^3/6E^2\end{cases}\tag{2}$$

where ψ is also can be found in this literature [38]. During the unloading phase, the constitutive relation between the contact force and displacement is expressed as

$$F(\delta)=\begin{cases}\dfrac{4}{3}ER^{\frac{1}{2}}\delta^{\frac{3}{2}} & \delta_{\max}<\delta_y\\ \dfrac{4}{3}E\left(R_{ep}^{e}\right)^{\frac{1}{2}}(\delta-\delta_r)^{\frac{3}{2}} & \delta_y\le\delta_{\max}<\delta_p\\ \dfrac{4}{3}E\left(R_{p}^{e}\right)^{\frac{1}{2}}(\delta-\delta_r)^{\frac{3}{2}} & \delta_{\max}\ge\delta_p\end{cases} \tag{3}$$

where R_{ep}^{e} is the radius of curvature after impact in the elastoplastic phase. R_{p}^{e} is the radius of curvature after impact in the plastic phase.

3. A new contact model applied to the granular system

The granular system often suffers from impact with high velocity, as well as from the situation where the material properties of the particle possess a large Young's modulus and small yield strength. The latter situation leads to the impact behavior being prone to activate elastoplastic or plastic deformations. Therefore, once the contact behavior comes into the elastoplastic or plastic phase, the relationship between the load and deformation can be treated as a linear, as shown in Fig. 1. Kelvin and Voigt are pioneers of the contact force model considering energy dissipation, which adopted a linear spring-damper model to represent the contact behavior between the contact bodies. This approach inspired us to propose a new contact force model based on a linear vibration system. However, the contact behavior must undergo the elastic phase prior to coming into the elastoplastic or plastic contact phase, and the elastic contact process governed by the Hertz contact law is a nonlinear behavior [67] in Fig. 1. It is difficult to derive the analytical solution of the damping coefficient if a nonlinear vibration system needs to be solved. Therefore, to avoid solving the nonlinear equation of motion, the assumption of the frequency-dependent damping in the elastic phase refers to the hypothesis regarding the viscous damping in the elastoplastic phase by a new loss factor. After obtaining the loss factors in the elastic and elastoplastic phase, the new contact force model with viscous damping factor, including the elastic, elastoplastic, and plastic phases, can be formulated based on the cornerstone of the Kelvin-Voigt contact model. Finally, the new contact force model not only completes the transition from the nonlinear elastic contact phase to the linear elastoplastic phase but also inherits the continuous properties from the ML model.

3.1. In the elastoplastic phase

The equation of motion can be written as

$$M\ddot{\delta}+D_1\dot{\delta}+K\delta=0 \tag{4}$$

where M is the mass of the contact body, D_1 is the frequency-dependent damping coefficient, K is the stiffness coefficient of spring. The

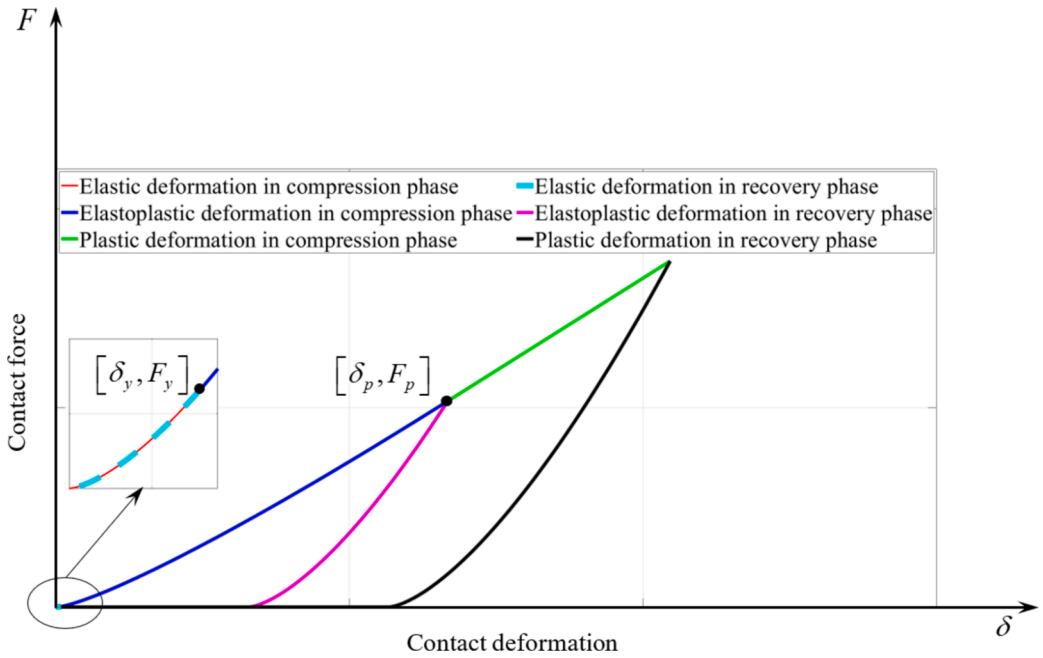

Fig. 1. Relationship between the force and deformation in the ML model.

frequency-dependent damping coefficient is assumed as[65]

$$D_1 = \frac{g_1 K}{\omega} = g_1\sqrt{KM} \tag{5}$$

where g_1 is the loss factor, ω is the natural frequency, $\omega = \sqrt{K/M}$. The solution to the underdamped system is expressed as

$$\delta(t) = Ae^{-\xi\omega t}\sin(\omega_d t + \phi) \tag{6}$$

where A is the amplitude, ϕ is the phase angle, ω_d is the damped frequency, $\omega_d = \omega\sqrt{1-\xi^2}$. ξ is the damping, $\xi = D_1/2M\omega = g_1/2$.

The amplitude and phase angle can be determined from the initial condition

$$\begin{cases} t = 0, \delta = 0 \Rightarrow 0 = \sin(\phi) \\ t = 0, \dot{\delta} = \dot{\delta}^{(-)} \Rightarrow \dot{\delta}^{(-)} = A\omega_d\cos(\phi) \end{cases} \Rightarrow \phi = 0, A = \frac{\dot{\delta}^{(-)}}{\omega_d} \tag{7}$$

where $\dot{\delta}^{(-)}$ is the initial impact velocity. Eq. (6) can be rewritten as

$$\delta(t) = \frac{\dot{\delta}^{(-)}}{\omega_d}e^{-\xi\omega t}\sin(\omega_d t)\omega_d = \omega\sqrt{1-\xi^2} = \frac{\omega}{2}\sqrt{4-g_1^2} \tag{8}$$

The duration time of the entire contact process is given by

$$t_1 = \frac{\pi}{\omega_d} = \frac{2\pi}{\omega}\left[4 - g_1^2\right]^{-\frac{1}{2}} \tag{9}$$

When an entire contact process terminates, the deformation in Eq. (10) is equal to zero, and the relative impact velocity is expressed as according to Eq. (8)

$$\dot{\delta}(t) = \frac{\dot{\delta}^{(-)}}{\omega_d}e^{-\xi\omega t}\left[-\xi\omega\sin(\omega_d t) + \omega_d\cos(\omega_d t)\right] \Rightarrow \dot{\delta}(t_1) = \dot{\delta}^{(-)}e^{-\xi\omega t_1} \tag{10}$$

According to the definition of Newton's coefficient of restitution (CoR), and substituting Eq. (9) into Eq. (10), the following equations can be written as

$$\begin{aligned} c_r = \frac{\dot{\delta}(t_1)}{\dot{\delta}^{(-)}} = \frac{\dot{\delta}^{(-)}e^{-\xi\omega t_1}}{\dot{\delta}^{(-)}} \Rightarrow c_r = e^{-\xi\omega t_1} \Rightarrow \ln c_r = -\xi\omega t_1 \\ \Rightarrow g_1 = 2|\ln c_r|\sqrt{\frac{1}{\pi^2 + \ln^2(c_r)}} \end{aligned} \tag{11}$$

Thereby, according to Eq. (4), the other new dynamic dashpot model in the elastoplastic or plastic phase can be written as:

$$F_{np} = K\delta + D_1\dot{\delta} = K_p\delta + g_1\sqrt{K_p M}\dot{\delta}K_p = \frac{F(\delta_p) - F(\delta_y)}{\delta_p - \delta_y} \tag{12}$$

where K_p is the linearized contact stiffness based on the ML model in Fig. 1.

3.2. In the elastic contact phase

At the beginning of the contact phase, elastic deformation is activated prior to the elastoplastic deformation in Fig. 1, which is governed by the Hertz contact law. According to Eq. (12), the contact force with frequency-dependent damping in the elastic phase is expressed as based on Hertz contact law

$$F_e = K_h\delta^{\frac{3}{2}} + D_2\dot{\delta} \tag{13}$$

It should be pointed out that the linear viscous damping coefficient does not conform to the requirement of the frequency-dependent damping in the elastic contact phase. Therefore, based on the assumption in Eq. (5), the nonlinear elastic damping coefficient is assumed as

$$D_2 = \frac{g_2 K_h}{\omega}\delta^{\frac{1}{4}} = g_2\sqrt{K_h M}\delta^{\frac{1}{4}} \tag{14}$$

Accordingly, the energy dissipation can be obtained by integrating Eq. (14) in the elastic contact phase

$$\Delta E = \int_0^{\delta_{\max}} D_2 \dot{\delta} d\delta = \int_0^{\delta_{\max}} g_2 \sqrt{K_h M} \delta^{\frac{1}{4}} \dot{\delta} d\delta \tag{15}$$

where $\delta_{\max}$ is the maximum contact deformation.

Based on the energy balance in the process of contact behavior, the dissipated energy can be written as [56,60]

$$\Delta E = \frac{1}{2} M \left(1 - c_r^2\right) [\dot{\delta}^{(-)}]^2 \tag{16}$$

The relative impact velocity is a crucial factor in obtaining the energy dissipation in Eq. (15); hence, to obtain the relative impact velocity, the stored strain energy from the elastic force is equated to the kinetic energy at the time of separation at the beginning of the recovery phase. It is expressed as

$$\int_0^{\delta_{\max}} K_h \delta^{\frac{3}{2}} d\delta = \frac{1}{2} M \dot{\delta}_f^2 \tag{17}$$

where $\dot{\delta}_f$ is the post-impact velocity. By solving Eq. (17), the maximum contact deformation can be expressed as

$$\delta_{\max} = \left(\frac{5}{4} \frac{M}{K_h} \dot{\delta}_f^2\right)^{\frac{2}{5}} \Rightarrow \dot{\delta}_f^2 = \frac{4K_h}{5M} \delta_{\max}^{\frac{5}{2}} \tag{18}$$

In the recovery phase, the elastic strain energy is transformed again into the kinetic energy; hence, which is described as:

$$\int_0^{\delta} K_h \delta^{\frac{3}{2}} d\delta + \frac{1}{2} M \dot{\delta}^2 = \frac{1}{2} M \dot{\delta}_f^2 \tag{19}$$

By solving Eq. (19), the relative impact velocity in the recovery phase ($\dot{\delta} < 0$) can be written as

$$\dot{\delta} = -\sqrt{\dot{\delta}_f^2 - \frac{4}{5} \frac{K_h}{M} \delta^{\frac{5}{2}}} \tag{20}$$

However, the relative impact velocity ($\dot{\delta} > 0$) in the compression phase cannot be directly obtained from Eq. (20). The loss of difference of velocities $\dot{\delta}^{(-)} - \left|\dot{\delta}_f\right|$ is assumed to be uniform during the whole compression phase. Therefore, the relative impact velocity in the compression phase can be written as [74]

$$\dot{\delta} = \sqrt{\dot{\delta}_f^2 - \frac{4K_h}{5M} \delta^{\frac{5}{2}}} + \frac{\left(\dot{\delta}^{(-)} - \left|\dot{\delta}_f\right|\right)(\delta_{\max} - \delta)}{\delta_{\max}} \tag{21}$$

Substituting Eq. (21) into Eq. (15), and combined with Eq. (16) gives the following expression

$$\frac{1}{2} M \left(1 - c_r^2\right) [\dot{\delta}^{(-)}]^2 = g_2 \sqrt{K_h M} \int_0^{\delta_{\max}} \delta^{\frac{1}{4}} \left[\sqrt{\dot{\delta}_f^2 - \frac{4K_h}{5M} \delta^{\frac{5}{2}}} + \frac{\left(\dot{\delta}^{(-)} - \left|\dot{\delta}_f\right|\right)(\delta_{\max} - \delta)}{\delta_{\max}}\right] d\delta \tag{22}$$

The post-impact velocity can be obtained from Eq. (18). The first term in the right-hand side can be written as

$$\begin{aligned} g_2 \sqrt{K_h M} \int_0^{\delta_{\max}} \delta^{\frac{1}{4}} \sqrt{\dot{\delta}_f^2 - \frac{4}{5} \frac{K_h}{M} \delta^{\frac{5}{2}}} d\delta &= g_2 \sqrt{K_h M} \int_0^{\delta_{\max}} \delta^{\frac{1}{4}} \sqrt{\frac{4K_h}{5M} \delta_{\max}^{\frac{5}{2}} - \frac{4}{5} \frac{K_h}{M} \delta^{\frac{5}{2}}} d\delta \\ &= \frac{2\sqrt{5}}{5} g_2 K_h \int_0^{\delta_{\max}} \delta^{\frac{1}{4}} \sqrt{\delta_{\max}^{\frac{5}{2}} - \delta^{\frac{5}{2}}} d\delta = \frac{2\sqrt{5}}{25} \pi g_2 K_h \delta_{\max}^{\frac{5}{2}} \end{aligned} \tag{22a}$$

Substituting Eq. (22a) into Eq. (22)

$$\frac{1}{2}M(1-c_r^2)[\dot{\delta}^{(-)}]^2=\frac{2\sqrt{5}}{25}\pi g_2 K_h \delta_{\max}^{\frac{5}{2}}+g_2\sqrt{K_h M}\,\frac{\left(\dot{\delta}^{(-)}-\left|\dot{\delta}_f\right|\right)}{\delta_{\max}}\int_0^{\delta_{\max}}\delta^{\frac{1}{4}}(\delta_{\max}-\delta)d\delta$$

$$\Rightarrow \frac{1}{2}M(1-c_r^2)[\dot{\delta}^{(-)}]^2=\frac{2\sqrt{5}}{25}\pi g_2 K_h \delta_{\max}^{\frac{5}{2}}+g_2\sqrt{K_h M}\,\frac{\left(\dot{\delta}^{(-)}-\left|\dot{\delta}_f\right|\right)}{\delta_{\max}}\left(\delta_{\max}\int_0^{\delta_{\max}}\delta^{\frac{1}{4}}d\delta-\int_0^{\delta_{\max}}\delta^{\frac{5}{4}}d\delta\right) \tag{22b}$$

$$\Rightarrow \frac{1}{2}M(1-c_r^2)[\dot{\delta}^{(-)}]^2=\frac{2\sqrt{5}}{25}\pi g_2 K_h \delta_{\max}^{\frac{5}{2}}+\frac{16}{45}g_2\sqrt{K_h M}\left(\dot{\delta}^{(-)}-\left|\dot{\delta}_f\right|\right)\delta_{\max}^{\frac{5}{4}}$$

Substituting Eq. (18) into Eq. (22b), and $\left(\dot{\delta}_f=c_r\dot{\delta}^{(-)}\right)$

$$\frac{1}{2}M(1-c_r^2)[\dot{\delta}^{(-)}]^2=\frac{2\sqrt{5}}{25}\pi g_2 K_h \delta_{\max}^{\frac{5}{2}}+\frac{16}{45}g_2\sqrt{K_h M}\left(\dot{\delta}^{(-)}-\left|\dot{\delta}_f\right|\right)\delta_{\max}^{\frac{5}{4}}$$

$$\Rightarrow \frac{1}{2}M(1-c_r^2)[\dot{\delta}^{(-)}]^2=\frac{2\sqrt{5}}{25}\pi g_2 K_h \frac{5}{4}\frac{M}{K_h}\dot{\delta}_f^2+\frac{16}{45}g_2\sqrt{K_h M}\left(\dot{\delta}^{(-)}-\left|\dot{\delta}_f\right|\right)\sqrt{\frac{5}{4}\frac{M}{K_h}\dot{\delta}_f^2}$$

$$\Rightarrow \frac{1}{2}M(1-c_r^2)[\dot{\delta}^{(-)}]^2=\frac{\sqrt{5}}{10}\pi g_2 M c_r^2[\dot{\delta}^{(-)}]^2+\frac{8\sqrt{5}}{45}g_2 M\left(c_r[\dot{\delta}^{(-)}]^2-c_r^2[\delta^{(-)}]^2\right)$$

$$\Rightarrow \frac{1}{2}(1-c_r^2)=\frac{\sqrt{5}}{10}\pi g_2 c_r^2+\frac{8\sqrt{5}}{45}g_2(c_r-c_r^2)\Rightarrow 9\sqrt{5}(1-c_r^2)=g_2(9\pi c_r^2+16c_r-16c_r^2) \tag{23}$$

$$\Rightarrow g_2=\frac{9\sqrt{5}(1-c_r^2)}{c_r[c_r(9\pi-16)+16]}$$

Therefore, in the elastic contact phase, the contact force model with frequency-dependent damping can be formulated as

$$F_e=K_h\delta^{\frac{3}{2}}+g_2\sqrt{K_h M}\delta^{\frac{1}{4}}\dot{\delta} \tag{24}$$

Finally, a complete contact force model with frequency-dependent damping can be expressed as

$$F=\begin{cases}K_h\delta^{\frac{3}{2}}+g_2\sqrt{K_h M}\,\delta^{\frac{1}{4}}\dot{\delta} & (\delta\le\delta_y)\\ K_p\delta+g_1\sqrt{K_p M}\,\dot{\delta} & (\delta>\delta_y)\end{cases} \tag{25}$$

The proposed dynamics contact model seems to just include the elastic and elastoplastic phases from its mathematical expression. However, since the elastoplastic phase has the same contact stiffness in Eq. (12) as the plastic phase, the contact force in the plastic phase can also be calculated using the second equation in Eq. (25). When the impact behavior comes into the plastic phase, the critical plastic deformation δ_p can serve as the criterion to differ the elastoplastic phase from the plastic phase.

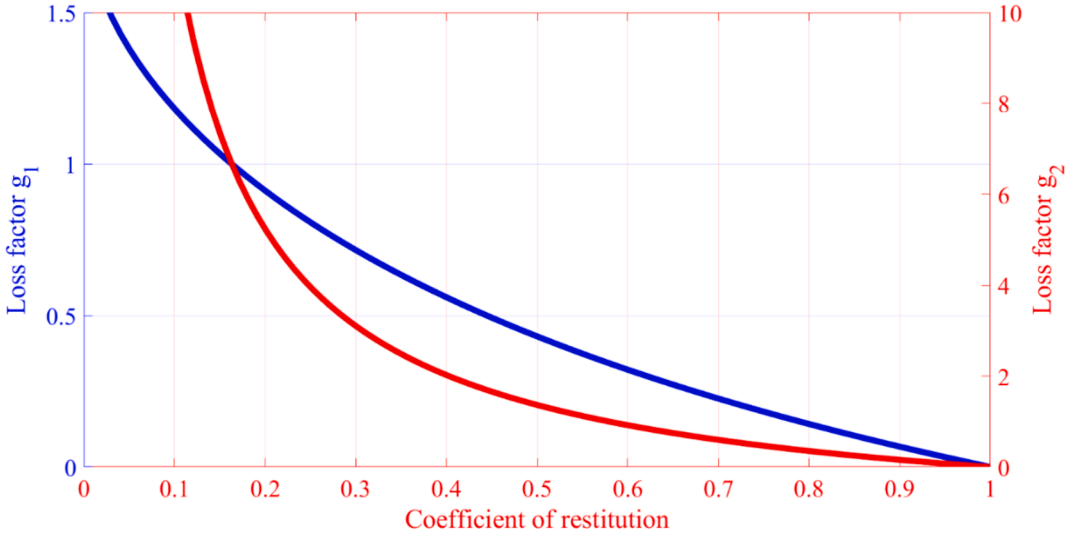

Fig. 2. Relationship between the loss factor and CoR.

Moreover, it is noteworthy that the new dynamic dashpot model in the elastic phase is almost the same as the dashpot model used in the EDEM software, which is expressed as [45]

$$F_{dem} = K_h\delta^{\frac{3}{2}} + \frac{\sqrt{5}}{2}g_1\sqrt{K_hM}\delta^{\frac{1}{4}}\dot{\delta} \tag{26}$$

This model is referred to as the EDEM contact model in this investigation.

3.3. Relationship between the loss factor and coefficient of restitution

The new contact force model hypothesizes that the damping coefficient in the different contact phases is a function of the frequency of the system. The development is made by introducing different loss factors, which are convenient to represent the energy dissipation during contact. The loss factors in Eq. (11) and Eq. (23) are determined by the CoR in Fig. 2. When the contact comes into the elastoplastic or plastic phase, the relationship between the load and deformation is almost linear in Fig. 1; the loss factor increases with the decrease of CoR. When the CoR is larger than 0.4, the relationship between the loss factor g_1 and CoR behaves approximately linear in the elastoplastic or plastic phase.

At the beginning of the impact behavior, the relationship between the contact force and deformation is nonlinear; therefore, the loss factor g_1 in Eq. (11) is no longer suited for nonlinear contact behavior. After this point, a nonlinear frequency-dependent damping behavior is assumed, as introduced in Eq. (14) by means of the assumption from the linear contact behavior in Eq. (5). The loss factor g_2 increases with the decrease of CoR as well. However, in the elastic phase, the energy dissipation caused by the seismic waves is very small, which causes the CoR to take a comparatively larger value. When the CoR is larger than 0.8, the relationship between the loss factor g_2 and CoR approximates a linear relationship. In other words, a larger loss factor leads to more energy being dissipated. The dissipated energy in the different contact phases is unified by means of the loss factors.

3.4. Dynamic performance of the new model

Considering that the new contact model is tailored to the granular system, the contact between two identical spheres is taken as the numerical example displayed in Fig. 3. The simulation parameters can be seen in Table 1. The dimensionless parameters are assumed according to values from the literature, i.e., $\psi = 3.0\varepsilon = 13$. The critical elastic deformation is equal to 5.2453E-6 m, and the critical plastic deformation is equal to 4.4323E-4 m. In this section, the dynamic performance of the new contact force model is tested under the different initial impact velocities in three different contact phases. To illustrate the tensile force area in the new contact force model and its high accuracy, the Hunt-Crossley model and the EDEM contact model are selected as the reference solutions. It is worth noting that the expression of the Hunt-Crossley contact model is written as

$$F = K_h\delta^{\frac{3}{2}}\left[1 + \frac{3(1-c_r)}{2}\frac{\dot{\delta}}{\dot{\delta}^{(-)}}\right] \tag{27}$$

The initial velocity of the first sphere is assumed to be 0.05 m/s; the second sphere is at rest initially. The relatively initial impact velocity is equal to 0.05 m/s. Under low impact velocity, the maximum contact deformation is smaller than the critical elastic deformation. The entire contact process is followed by the Hertz contact law. In the elastic phase, the energy dissipation during contact is negligible. Accordingly, the CoR is assumed as 0.95 in the new contact model. The dynamic responses obtained from the new contact model are entirely in agreement with the results calculated by the EDEM contact model in Fig. 4 when the CoR is equal to 0.9 in Eq. (26). The new contact model can completely reproduce the EDEM model in the elastic phase. Although the new contact model is inspired by the Kelvin-Voigt Model, it does not suffer from the deficiency of the Kelvin-Voigt Model. As for this deficiency, the relatively non-zero initial impact velocity between the contact bodies would lead to the contact force being equal to zero at the beginning of the contact phase.

Moreover, the post-impact velocity with inverse direction results in the contact force is equal to a negative value at the end of the recovery phase. However, as for the new contact force model and EDEM contact model, the viscous damping loop still starts from zero and goes back to zero in the entire contact process in Fig. 4 (a). This feature owes to the contribution of contact deformation in viscous damping. That is mainly explained by the effect of the viscous damping in Eq. (24) and Eq. (26), which circumvents the situation where the contact force has a positive value at the beginning of the contact event when the contact deformation is equal to zero. Moreover, at the beginning of the compression and at the end of recovery, the relative impact velocity is very large, compared to the Hunt-Crossley

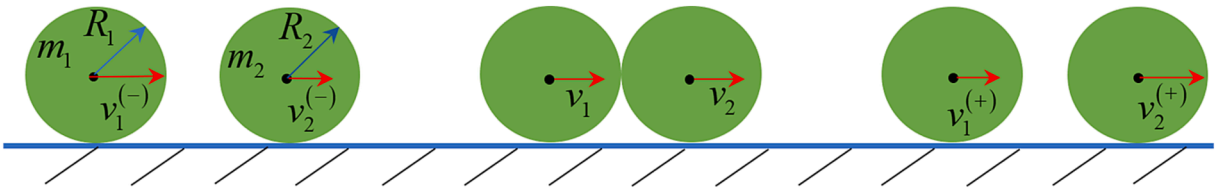

Fig. 3. One-dimension contact behavior between two particles.

Table 1
Contact parameters.

Element	Young's modulus (Pa)	Poisson ratio	Radius (m)	Yield strength (Pa)	Density (kg/m^3)
Body 1	2.07E11	0.30	2.0E-2	1.03E9	7800
Body 2	2.07E11	0.30	2.0E-2	1.03E9	7800

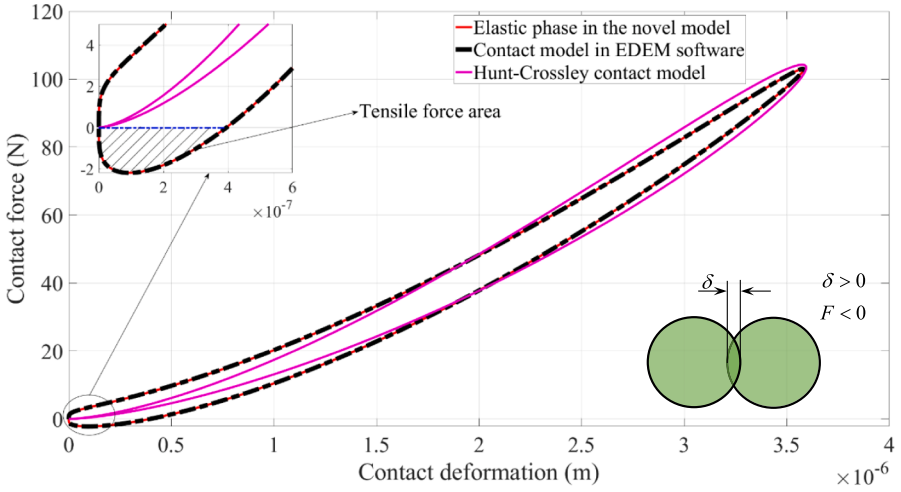

(a)

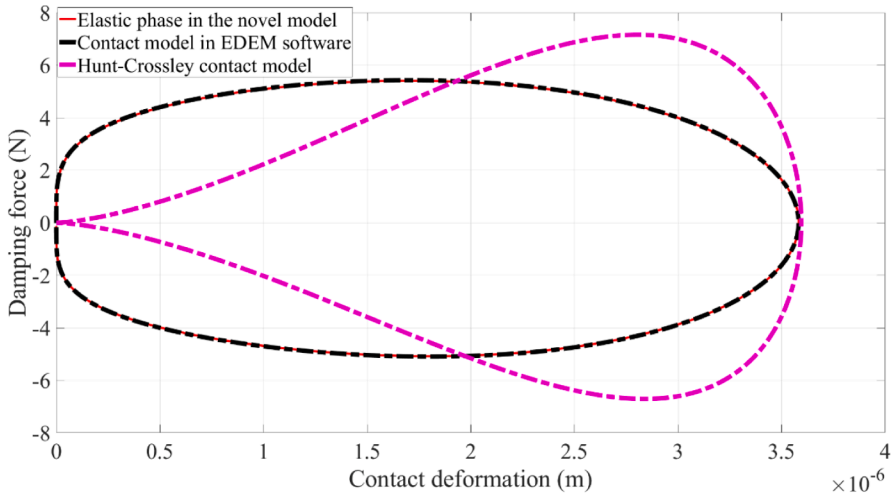

(b)

Fig. 4. Dynamic performances of the contact behavior under low impact velocity.

model; this situation creates a dramatic increase of the contact force at the beginning of compression, and an extreme decrease of this force at the end of the recovery phase.

Therefore, at the end of the recovery phase, the relative post-impact velocity reaches the maximum value (−0.04512 m/s) in Fig. 4 (c), which is almost the same with the post-impact velocity (−0.045 m/s) obtained by the definition of Newtonian's CoR. The post-impact velocities evaluated from three discrepant contact force models keep consistent with each other. Further, in Fig. 4 (a), the energy dissipation (5.1120E-5 J) calculated by three different contact models is very close to each other. This situation accounts for the proposed contact force model is capable of accurately describing the dissipated energy during impacy in the elastic phase. Moreover, the damping force in Fig. 4 (b) is larger than the elastic force; this leads to a situation where the viscous damping loop generates the

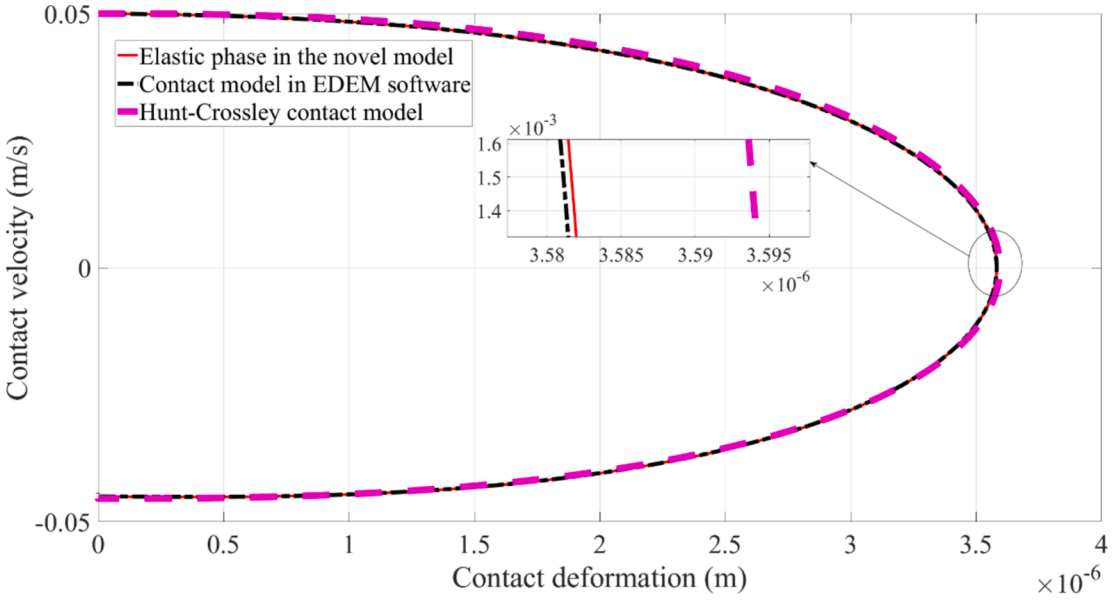

Fig. 4. (*continued*).

tensile force area in Fig. 4 (a). It is worth noting that another part of the tensile force area is that the contact deformation term makes the damping force larger than the Hunt-Crossley model at the beginning of compression and the end of the recovery phase Fig. 4 (b).

On the contrary, the Hunt-Crossley model employs a hysteresis damping factor to represent the energy dissipation, which effectively is frequency-independent damping. The hysteresis loop starts from zero and ends at zero as well in Fig. 4 (a). The relative contact deformation is smaller in the first half of the compression phase; the relative impact velocity is, on the other hand, comparatively large. In Fig. 4 (b), the damping force obtained from the new contact force model is larger than the damping force calculated by the Hunt-Crossley model because of the contact deformation term $\delta^{0.25}$ in the viscous damping coefficient.

In the second half of the recovery phase, a similar situation happens, which is the primary reason that the viscous damping loop produces the tensile force area. Conversely, the hysteresis loop has no tensile force area. It should be noted, however, that the contact force models with frequency-independent damping, like the Hunt-Crossley model, are not suited for simulating a granular system because most particles in the granular system are at rest initially. However, the denominator of the hysteresis damping factor includes the initial impact velocity. This could lead to serious numerical issues when the initial impact velocity approaches zero. Furthermore, when the CoR is equal to 0.9, the energy dissipation from the Hunt-Crossley model is almost consistent with the new contact model and EDEM contact model in Fig. 5 (a). Therefore, the maximum contact force in Fig. 5 (a) and post-impact velocity in Fig. 5 (c) from the different contact models are consistent with each other.

When the relative contact velocity is equal to 8 m/s, the maximum contact deformation is larger than the critical elastic and smaller than the critical plastic deformation. The elastoplastic contact behavior controls the entire contact process. In the elastic phase, the CoR is treated as 0.86; when the contact behavior comes into the elastoplastic phase, the CoR is equal to 0.70. Moreover, the CoR in the EDEM contact model and Hunt-Crossley model is also equal to 0.70. The tensile force area still exists in the viscous damping loop of the new contact force model and EDEM contact model. The Hunt-Crossley model with frequency-independent damping has no tensile force area. As for the new contact force model, it undergoes the elastic phase (red line) and elastoplastic phase (green line) in sequence in Fig. 5. Obviously, compared to the EDEM contact model, the contact force obtained from the new contact force model decreases after experiencing the elastic contact phase. That is mainly because the EDEM contact model employs the Hertz contact stiffness to represent the contact stiffness in the elastoplastic phase, which overestimates the contact force in the elastoplastic phase [50], no matter what the contact behavior is included in the compression or recovery phase in Fig. 5 (a). Likewise, the Hunt-Crossley model shows the same behavior as the EDEM contact model. The new contact force model utilizes the relationship between the load and deformation in the ML model to derive the contact stiffness in the elastoplastic phase.

In Fig. 5 (a), the damping loops generated by three different contact force models represent the energy dissipation during impact. Since the ML model is almost consistent with the experimental data [38], it is treated as the reference solution of energy dissipation during impact. The evaluation of energy loss from three different contact force models can be seen in Table 2. Consipciously, the energy dissipation from three different contact force models has a deviation from the ML model, but overall, they are relatively close to each other. Consequently, the new contact force model can precisely describe the energy dissipation during impact.

In the elastic phase, the EDEM contact model is almost identical to the new contact force model in Fig. 5 (b) because the Hertz contact law governs their behavior. Once the contact event comes into the elastoplastic phase, the damping force obtained from the new contact force model is smaller than the damping force from the EDEM contact model, which is also caused by the Hertz contact stiffness in the EDEM contact model. In Fig. 5 (c), the post-impact velocities from three different contact force models are very similar

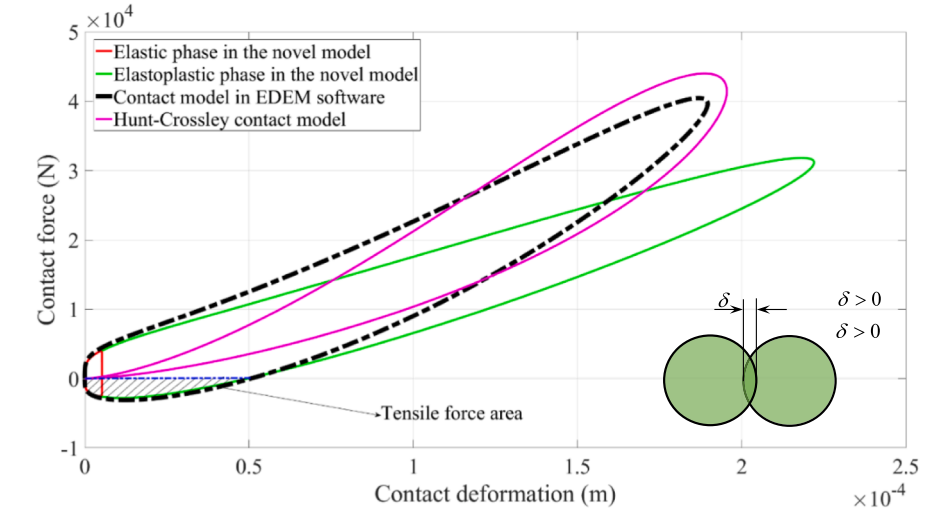

(a)

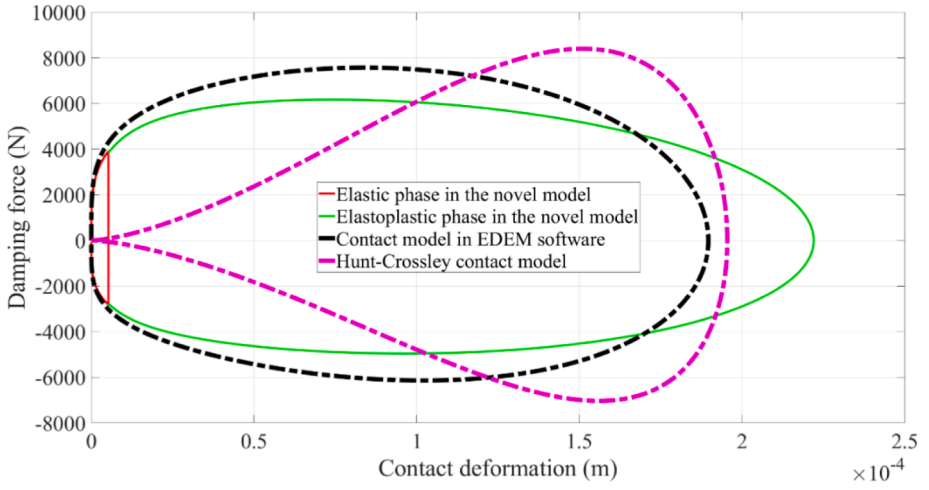

(b)

Fig. 5. Dynamic performances of the contact behavior when the elastoplastic deformation is activated.

despite the maximum contact forces between them being different from each other. Further, the post-impact velocity calculated by the proposed contact force model is equal to −5.75541 m/s, which is very close to the post-impact velocity (−5.6 m/s) obtained by the definition of Newtonian's CoR. Accordingly, this phenomenon also proves that the proposed contact force model is able to precisely depict the dissipated energy during impact in the elastoplastic contact phase.

When the initial velocity increases to 25 m/s, the contact behavior comes into the full plastic phase. Likewise, in the elastic phase, the CoR equals 0.84; when the plastic deformation is activated, the CoR is equal to 0.65, which is also suited for the EDEM contact and Hunt-Crossley models. In Fig. 6, when the plastic phase is activated, the contact behavior experiences the elastic phase (red line), elastoplastic phase (green line), and full plastic phase (blue line).

More importantly, the deviation caused by the Hertz contact stiffness between the EDEM contact model and the new contact model is more significant. However, the contact responses obtained from the new contact force model are still the same as the EDEM contact model in the elastic contact phase in Fig. 6 (b). The tensile force area still exists at the end of the recovery phase for both contact models in Fig. 6 (a). Moreover, when the elastoplastic or plastic phase is activated, the contact stiffness is smaller than the Hertz contact stiffness. This explains why the contact deformation from the new contact force model is larger than the one predicted by the Hunt-Crossley model and EDEM contact models. The post-impact velocity calculated by the Hunt-Crossley model has an apparent deviation from the EDEM contact model and the new contact force model in Fig. 6 (c).

In Fig. 6 (a), when the plastic deformation is activated, the evaluation of energy loss from three different contact force models can

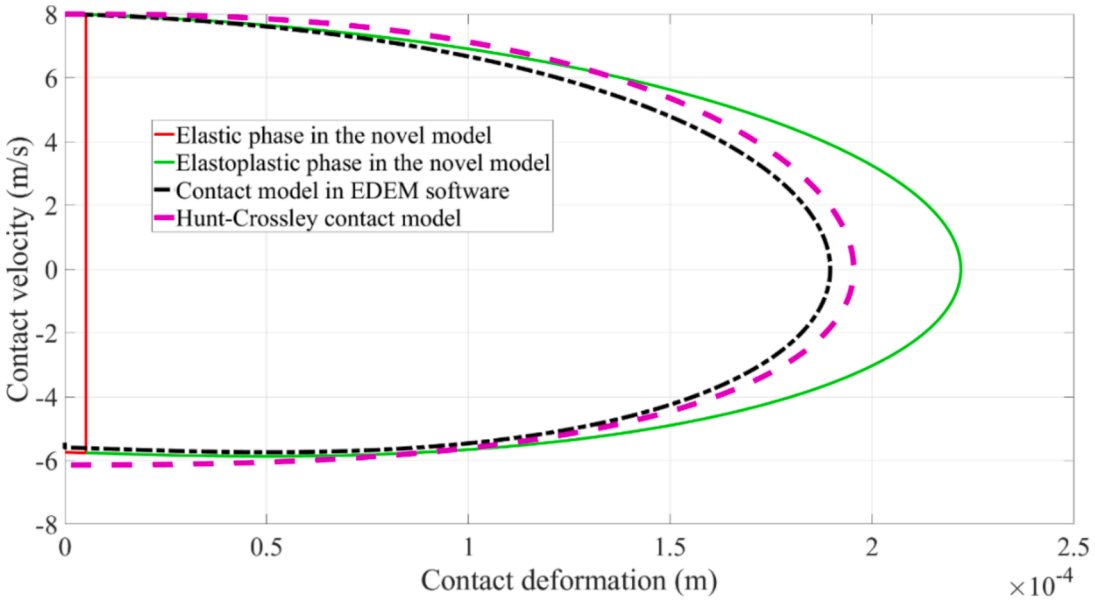

Fig. 5. (*continued*).

Table 2
Energy dissipation in the elastoplastic phase.

Parameters Model	ML model	Hunt-Crossley model	EDEM model	New model
Loss energy ΔE(J)	1.9381	1.7109	2.0389	2.0710
Error percentage ΔE	——	11.72 %	5.21 %	6.86 %

be seen in Table 3. Consipciously, the Hunt-Crossley model is incapable of precisely calaulating the energy dissipation during impact in the plastic phase. Nevertheless, compared to the ML model, the error percentage of energy loss generated by the EDEM model is slightly smaller than the one from the proposed contact force model. Thereby, the new contact force model is capable of describing the energy dissipation during impact. However, it is important to note that the EDEM contact model cannot attain accurately the maximum contact deformation and contact force because it adoptes the Hertz contact stiffness coefficient.

Based on the definition of Newton's CoR, the post-impact velocity should be equal to the initial impact velocity multiple the CoR, which is equal to 16.25 m/s. The post-impact velocity calculated by the new contact force model or the EDEM contact model equals 16.22 m/s. This conclusion also illustrates the proposed contact force model can evaluate the energy dissipation during impact in the plastic phase. However, the post-impact velocity obtained from the Hunt-Crossley model is equal to 18.58 m/s. This conclusion accounts for the fact that the Hunt-Crossley model lost control of energy dissipation when the contact is introduced into the plastic phase. This means that the Hunt-Crossley model is only suited for the low-impact velocity scenario. On the other hand, frequency-dependent damping is better at describing the energy dissipation during contact compared to frequency-independent damping.

3.5. Comparison between the ML model and the new contact model

As for the ML model, the loading path is the same as the unloading path in the elastic phase; there is no energy to be dissipated in the elastic phase. When the contact reaches the elastoplastic or full plastic phase, the loading path differs significantly from the unloading path. The closed area between the loading and unloading paths represents the energy dissipation during contact in Fig. 7. The static elastoplastic contact model can effectively recognize the maximum and residual contact deformation. Therefore, when using the static elastoplastic contact model to simulate the dynamic responses of the granular system, the maximum, and residual contact deformation must be identified and saved in every single contact as preparation for the ensuing contact behavior. This complicated calculation strategy is impossible when facing a massive number of particles. This is why the static elastoplastic contact models are not used in the EDEM software; in spite of that, they can accurately calculate the dynamic performances between the particles in the granular system. In light of this reason, the EDEM contact model in Eq. (26) is widely used in the EDEM software because it uses the viscous damping loop to represent the energy dissipation rather than the difference between the loading path and unloading path. This feature simplifies the calculation process of the static elastoplastic contact model in simulating the elastoplastic contact event. Namely, the EDEM contact model does not distinguish that the contact behavior is in the compression or recovery phase and does not calculate the maximum and residual contact deformations in every contact. This model just needs to check whether or not the contact behavior happens or not. Although the EDEM contact model extremely simplifies the calculation strategy of the elastoplastic contact behavior in

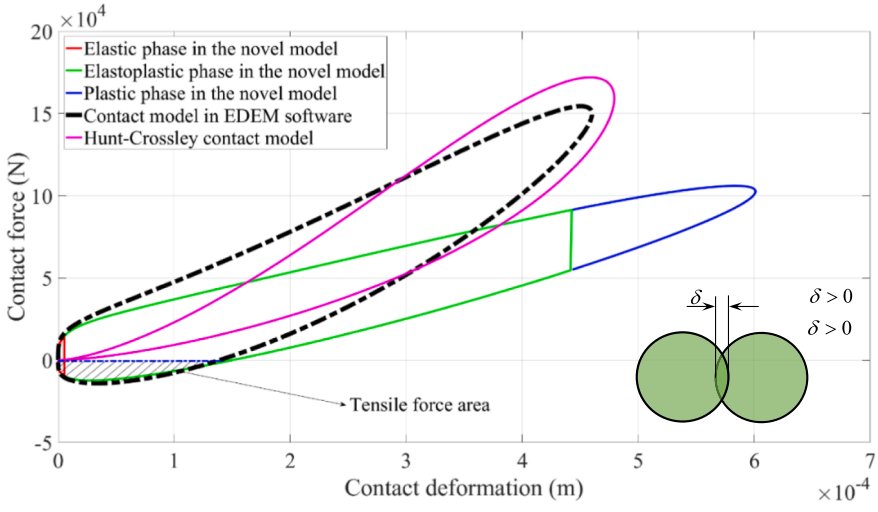

(a)

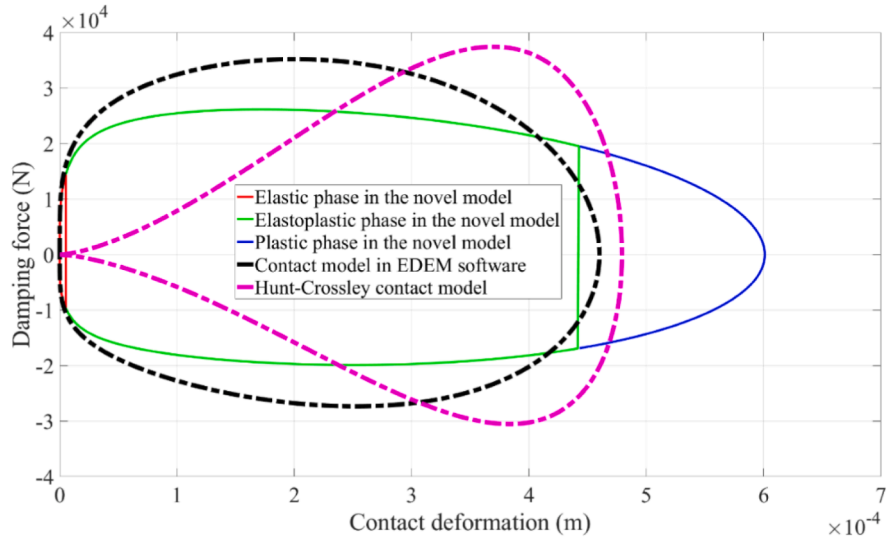

(b)

Fig. 6. Dynamic performances of the contact behavior when the plastic deformation is activated.

the granular system, the Hertz contact stiffness in the EDEM contact model amplifies the contact stiffness in the elastoplastic or plastic phase [50]. That is why we need to develop a new contact model.

Actually, the CoR can be identified as 0.65 by the ML model when contact behavior comes into the plastic phase under the initial impact velocity equal to 25 m/s. The new contact model has three different contact phases that correspond to the ML model. However, in the elastic contact phase, the energy dissipation caused by the seismic waves is considered using the viscous damping loop (red line). When the contact reaches the elastoplastic or plastic phase, the energy dissipation represented by the viscous damping loop corresponds to the closed area between the loading path and the unloading path. In order to bypass the effect of the tensile force area, we need to detect whether or not the contact force has a negative value in each time step. In Fig. 7, the contact force is forced to zero once it is smaller than zero. That is required since the occurrence of tensile force violates the physical meaning of the contact event between the particles in the granular system. It is worth noting that the new contact force model cannot be used to identify the residual contact deformation in the elastoplastic contact behavior. Point *A*, corresponding to the contact deformation, is caused by the tensile force area in the viscous damping loop. Point *B* from the ML model is the actual residual contact deformation in the elastoplastic contact behavior. In additional to this, the proposal contact model can judge which phase should be considered using the critical elastic and plastic deformation (the red line represents the elastic contact phase; the green line represents the elastoplastic contact phase; the blue line is the full plastic contact phase).

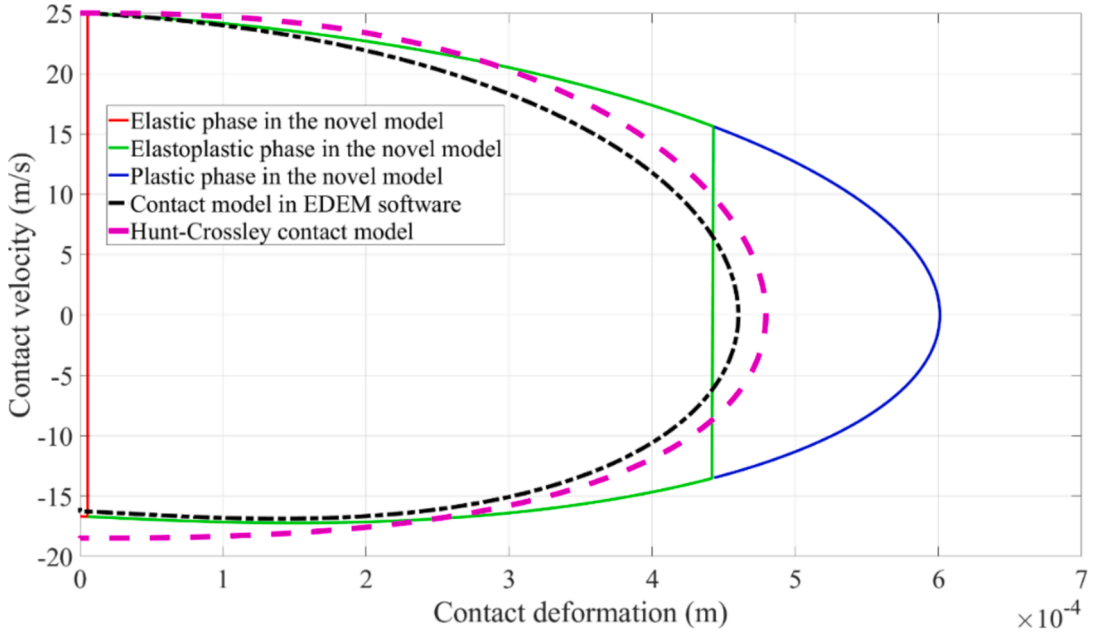

Fig. 6. (*continued*).

Table 3
Energy dissipation in the plastic phase.

Parameters Model	ML model	Hunt-Crossley model	EDEM model	New model
Loss energy ΔE(J)	24.7119	18.4735	22.5590	26.9543
Error percentage ΔE	——	25.24 %	8.71 %	9.07 %

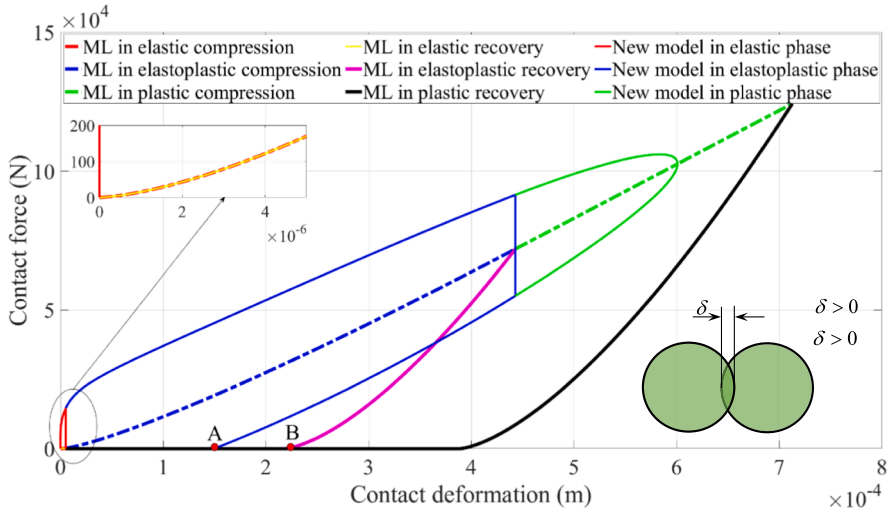

Fig. 7. Comparison analysis between the new contact model and ML model.

3.6. Bouncing ball example

A classical bouncing ball example [61] shows in Fig. 8. The radius of the ball is equal to 0.1 m; its mass is 1 kg. The initial height with respect to the ground is assumed as 1 m. The initial impact velocity is equal to 5 m/s. In the simulation process, the absolute error is set to be 2E-7. The integral strategy adopts the predictor–corrector method. The predictor is the Euler integrator. The corrector is the

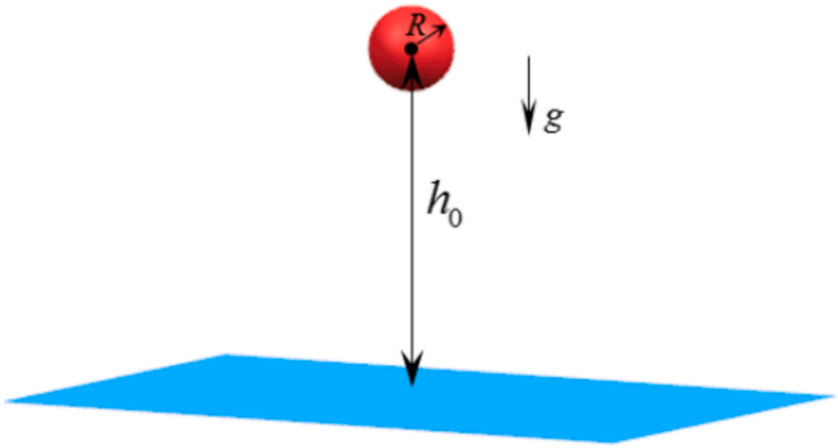

Fig. 8. Bouncing ball example [61].

trapezoidal integrator. When the contact behavior in the bouncing ball example is treated as an elastic collision only considering the energy dissipation caused by the transmission of the seismic waves. Namely, the initial kinetic energy of the bouncing ball needs around 7.5 s to be completely died out in Fig. 9 (blue dashed line is taken from reference [61]) because the seismic waves just dissipate very little energy in each contact between the sphere and ground. In order to check that the proposed contact model is capable of calculating the plastic collision event, Young's modulus of the ball is equal to 6.7e10 Pa; its Poisson ratio is equal to 0.33; its yield strength is equal to 2.4e7 Pa. The CoR is equal to 0.9 in the elastic phase; the CoR is assumed as 0.85 in the plastic phase.

In sharp contrast to the elastic contact, when the plastic deformation is activated in the bouncing ball example, the initial kinetic energy is fully dissipated caused by the plastic deformation in 2.5 s. That is because the plastic contact behavior dissipates more energy than the elastic contact behavior from the reference[61]. This application case adequately illustrates that the new dynamic dashpot model can be used for plastic impact events.

4. Granular system

The granular system is an exciting state of matter, which generally consists of spherical particles. It often emerges in the representation of complex linear and nonlinear solitary wave features. Although simple physical laws can describe the interaction between the particles, it is not easy to accurately reproduce the solitary wave in a granular chain. One-dimensional granular systems provide an abundant amount of information for contact mechanics. To validate the effectiveness and accuracy of the new contact force model, vertical and horizontal granular chains are taken as numerical examples to show the merit of the new contact force model in the granular chain.

4.1. Vertical granular chain

Fig. 10 depicts the experimental rig of the one-dimension vertical granular chain. The specific structure of this system can refer to the literature [869293]. The radius of a magnetic steel ball is equal to 2.5 mm and its mass is equal to 0.5115 g. The radius of the grain is equal to 2.38 mm. The material properties are displayed in Table 4. There are two different cases to exhibit the propagation of solitary waves under the different contact conditions: (i) Case 1: the mass of the particle is equal to 0.47 g, the magnetic force is equal to zero, and the dimensionless contact parameters ψ and ε are equal to 2.84 and 13. (ii) Case 2: the mass of the particle is equal to 1.23 g, the magnetic force is equal to 2.38 N, the dimensionless contact parameters ψ and ε are equal to 2.6 and 21, respectively. The striker velocity is equal to 0.44 m/s in both cases. The simulation time is 450 μs. The time step is 0.03 μs. The employed integrator is Matlab's builtin Ode45 solver.

Concerning Case 1, considering that this scenario happens under low impact velocity and without preload force, the energy dissipation during the whole contact process is negligible. Accordingly, in the elastic phase, the CoR is equal to 0.99. When the elastoplastic phase is activated, the CoR becomes equal to 0.93. The propagation of solitary waves can be seen in Fig. 11. To observe the solitary waves in Fig. 11, the contact force values of the 13th particle and the base are moved 25 N and −30 N along the Y axis, respectively. Significantly, in the first curve, the contact force applied on the 13th particle is propagated as a solitary wave. The curve of the 17th particle has a similar propagation to the first curve. However, the distance between the peak values is shorted because the contact behavior becomes more frequent when the particle approaches the base in the vertical granular chain. When the solitary wave arrives at the base, it is rebounded by the base to form the reflected wave in the third curve of Fig. 11. Moreover, its amplitude is the largest because of the effect of the gravity of the particles.

The new contact model can unambiguously reveal the solitary wave propagation in the vertical granular chain. The solitary waves obtained using the new contact model are consistent with the experimental data. Moreover, the model predictions stay consistent with the results from the ML model and EDEM contact models. This conclusion fully illustrates the correctness and accuracy of the proposed

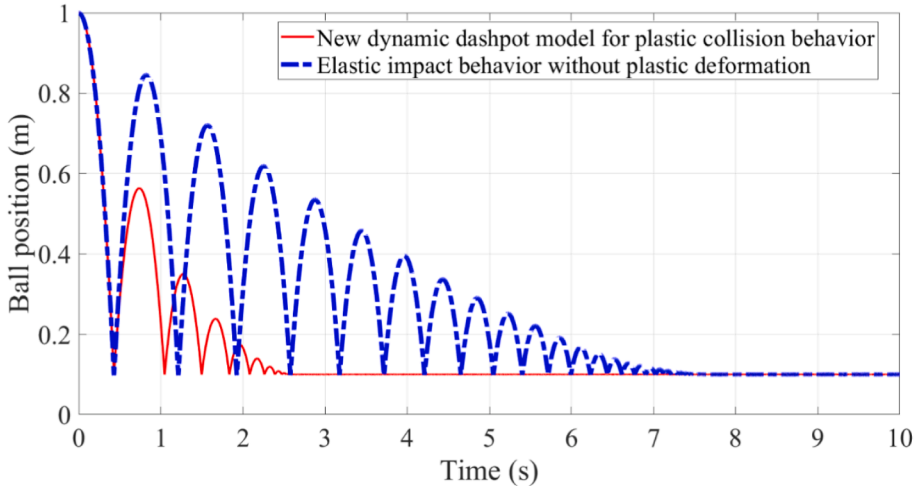

(a)

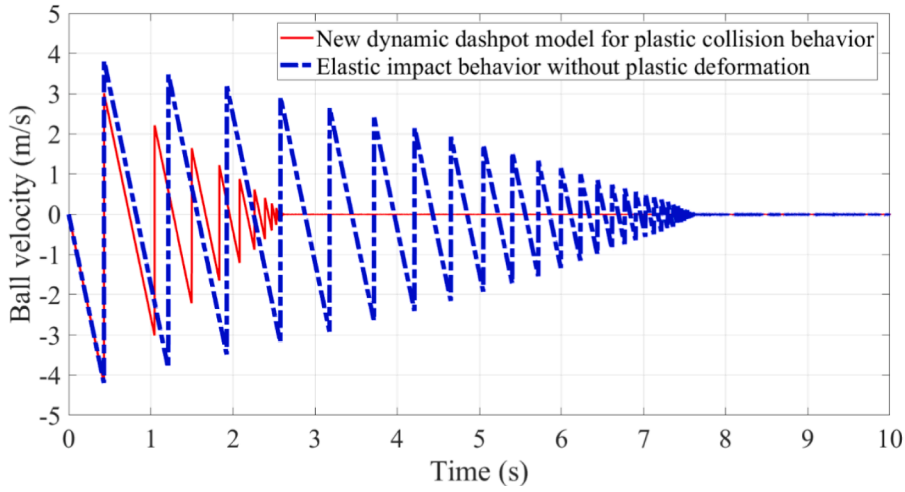

(b)

Fig. 9. Bouncing ball numerical example.

contact model.

Compared to the ML model, the new contact model simplifies the elastoplastic contact behavior calculation process because it does not identify the compression or recovery phase and saves the maximum and residual contact deformation from preparing for the next contact. Compared to the contact model applied in the EDEM software, although the solitary waves evaluated by the new contact model are closer to the experimental data, the difference between them is slight. That is mainly because, under low impact velocity and without preload force, the elastic contact dominates the entire impact between the particles despite the elastoplastic contact being activated.

Therefore, the discrepancy between the new contact model and the EDEM contact model is very small. In the horizontal granular chain, the distinction between them will be explained in detail. The error analysis between the numerical solutions and experimental data can be seen in Fig. 12. Conspicuously, the solitary waves obtained from the ML model are close to the experimental data compared to the other two contact models. Furthermore, the numerical solutions attained from the new contact force model are more accurate than the contact model applied in EDEM software, apart from the third curve caused by impacting the base in the vertical granular chain. The main reason is that the elastic behavior dominates this impact event despite the activation of the elastoplastic phase. That is why the error between the contact model used in EDEM software is smaller than the solution from the new contact model. Still, this error can be accepted compared to the magnitude of the peak value of the solitary waves.

As for Case 2, the impact experiment is implemented under the preload force generated by the magnet. The CoR in the elastic phase is equal to 0.98. When the contact comes into the elastoplastic phase, the CoR is equal to 0.87. The precompression leads to the

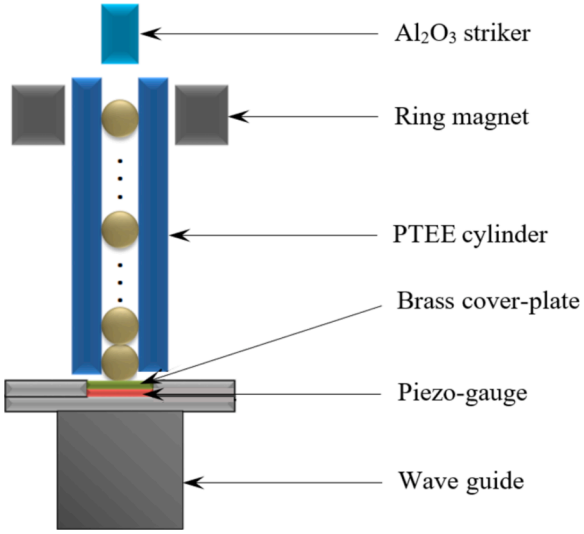

Fig. 10. The experimental setup of the vertical granular chain [39].

Table 4
Material parameters.

Material	Young's modulus	Poisson's ratio	Yield stress
Stainless steel 316	193 GPa	0.300	940 MPa
Red brass	115 GPa	0.307	250 MPa
Al_2O_3 aluminum	416 GPa	0.231	500 Mpa

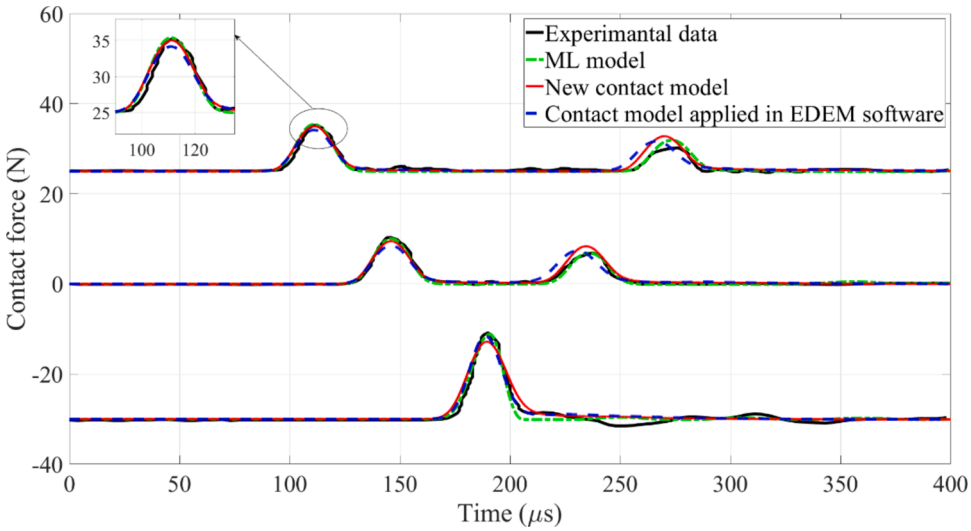

Fig. 11. The solitary wave in the vertical granular chain without magnetic force.

amplitude of solitary waves being larger when compared with those reported in Case 1, apart from the effect of the gravity of the particle. Furthermore, the propagation speed of solitary waves has been accelerated conspicuously because the wave speed depends on the peak value. Therefore, multiple impacts and multiple compression are observed in the vertical granular chain because of the different propagation speeds from the different particles. The contact behavior Case 2 is, as such, more complex than Case 1. In Fig. 13, the proposed contact force can reproduce the propagation of solitary waves, which basically coincides with the waves obtained from the ML model and EDEM contact model. However, the difference between the numerical solutions and experimental data is more significant than in Case 1. This is to be expected because reflection phenomena and multiple contact behavior are more frequent. In addition, the deviation between the EDEM contact model and experimental data is more significant when compared to Case 1. That is

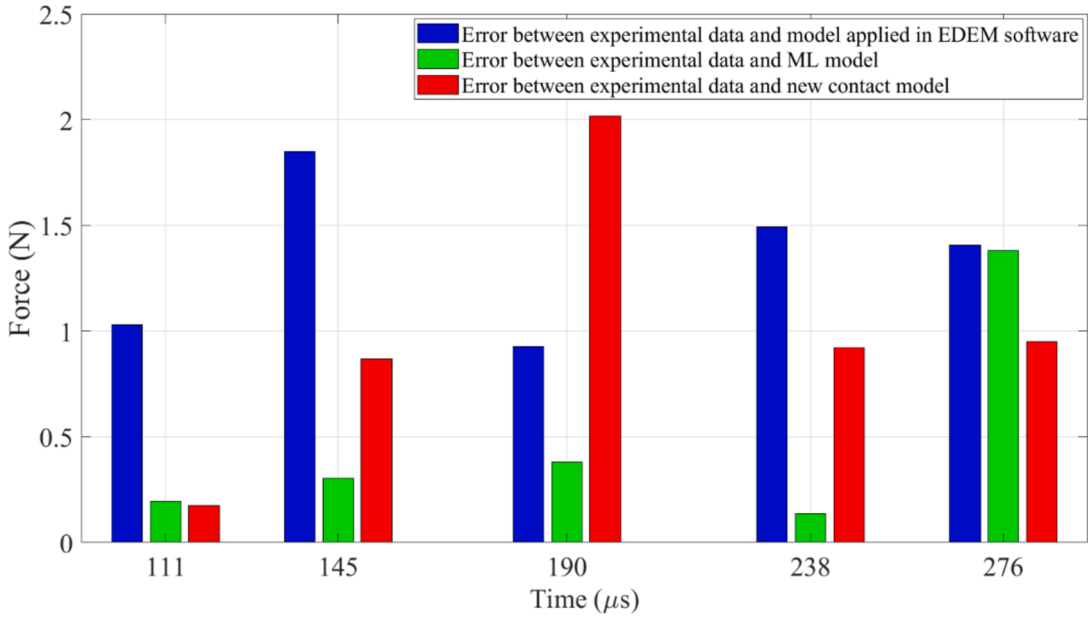

Fig. 12. The error analysis of the peak values in the solitary waves for the vertical granular chain.

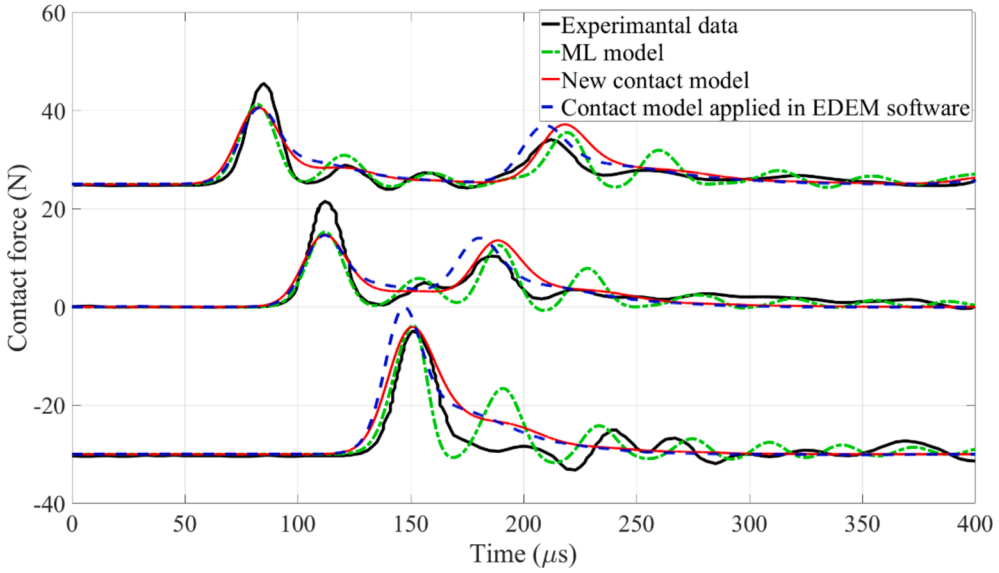

Fig. 13. The solitary wave in the vertical granular chain with magnetic force.

mainly explained by the magnetic force making the elastoplastic contact behavior dominate the entire contact process. Further, the EDEM contact model overestimates the contact stiffness in the elastoplastic contact event by the Hertz contact law [50].

This explains why the EDEM contact model has a significant error compared to the new contact model. More importantly, in Fig. 9 and Fig. 10, we found that the tensile force at the end of the recovery phase in the new contact model in Fig. 5 (a) does not affect the propagation of solitary waves in the granular chain. To further study this phenomenon, the relationship between the contact force and deformation regarding the 13th particle, 17th particle, and the base is reproduced in Fig. 14 (a)~(c). Obviously, the 13th and 17th particles demonstrate the multiple impacts and multiple compression phenomena during the entire contact process. As for both contact models, including the new contact model and EDEM contact model, at the end of the recovery phase, the magnitude of contact force is too small to affect the solitary wave propagation, although the 13th particle in Fig. 14 (a) generates the tensile force.

In addition to these observations, the tensile force area regarding the 13th particle can be ignored compared to the entire contact process because it just happens in a very short time at the end of the recovery phase. In Fig. 14 (b), as for the EDEM contact model, the tensile force on the 17th particle does not happen at the end of the recovery phase. The contact force almost starts from zero and ends at

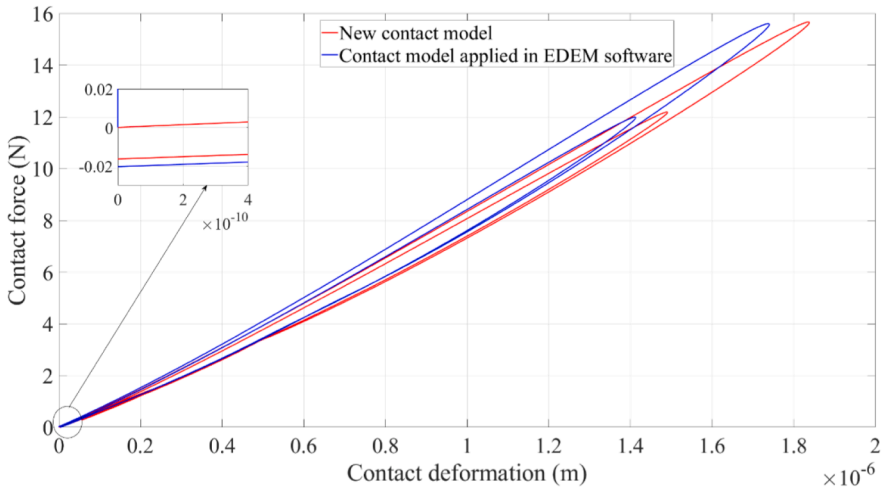

(a)

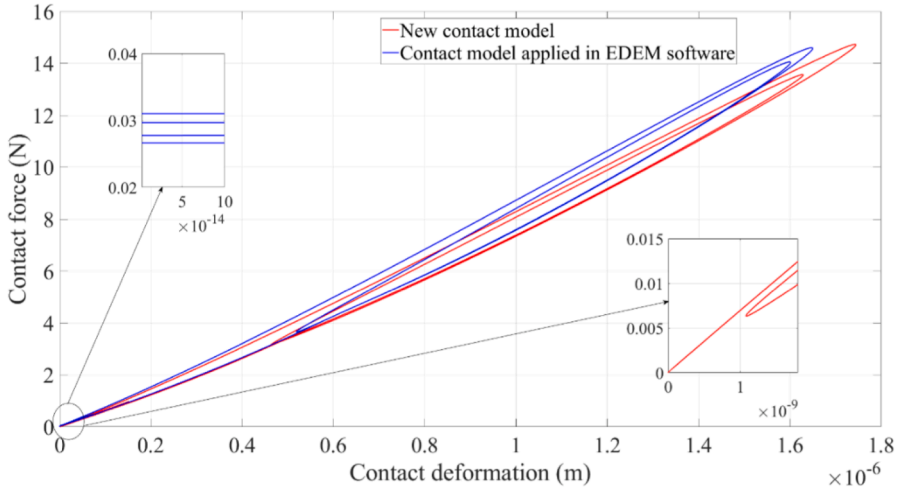

(b)

Fig. 14. The relationship between the contact force and deformation in the granular chain.

zero as well. However, in the new contact model, the production of the tensile force at the end of the recovery phase is prevented significantly due to the multiple compression and multiple impact phenomena. That is because the multiple impacts and multiple compression events in the recovery phase reduce the magnitude of the post-impact velocity or change the direction of the post-impact velocity. This again leads to the damping force at the end of the recovery phase becoming very small. That is why the contact force model with the viscous damping factor can describe the solitary wave propagation despite the tensile force area being included in the entire contact process. The multiple impacts and multiple compression phenomena almost eliminate the tensile force area in the granular system. When the solitary wave propagates to the base, the multiple impact and multiple compression are not significant compared to the 13th and 17th particles in Fig. 14 (c) because the primary function of the base is to reflect the solitary waves in the vertical granular chain. However, as for the new contact model, the micro-compression and micro-impact can be observed at the end of the recovery phase, which has the same ability as the multiple compression and multiple impact behavior in Fig. 14 (b) to stop the contact force from reaching into the tensile force area. Similarly, as for the EDEM contact model, the contact force, like the 13th particle in Fig. 14 (b), almost starts from zero and ends at zero.

In other words, the reason that the contact force model with frequency-dependent damping can be successfully used to produce solitary wave propagation lies in the notion that multiple impacts and multiple compression behaviors are prone to be generated in the granular chain. These behaviors prevent the contact force between the particles from diverging into the tensile force area. This investigation explains for the first time why the tensile force in the contact model with viscous damping has no effect on the dynamic

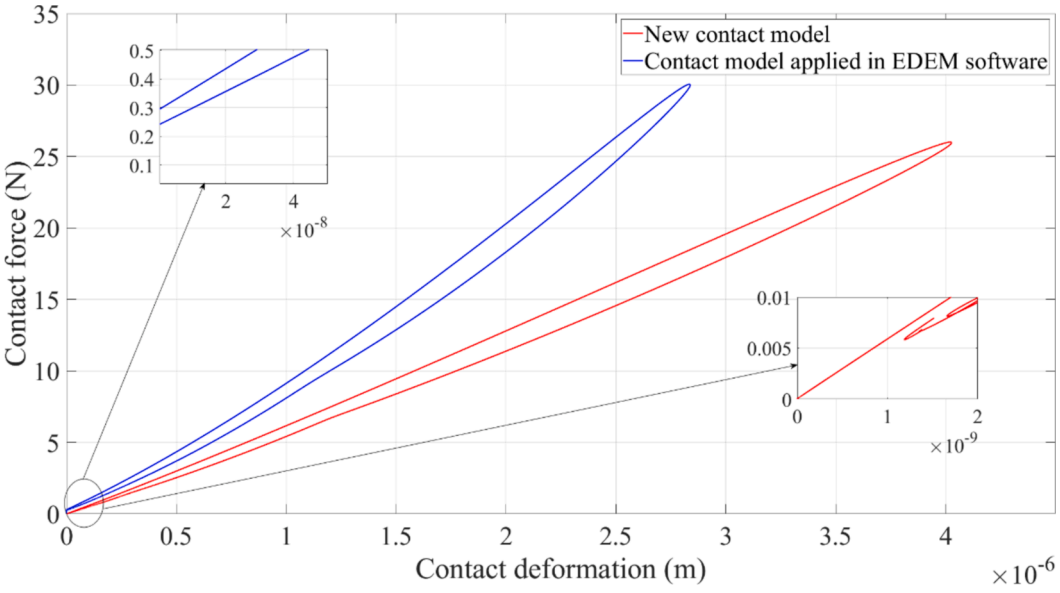

Fig. 14. (*continued*).

simulation in the granular system.

4.2. Horizontal granular chain

In the vertical granular chain, since the initial impact velocity of the striker is small, the high accuracy of the proposed contact model in allusion to the EDEM contact model is not highlighted significantly in Fig. 11 and Fig. 13. Therefore, in this section, a horizontal granular chain, as illustrated in Fig. 15, is selected to show the accuracy and effectiveness of the new contact force model. The initial impact velocity of the striker is set to 1.77 m/s. The experimental setup of a monodisperse granular chain of 70 stainless steel particles in Fig. 13 is originally designed by Daraio and coworkers [39,94]. The particle size and material properties are identical to each other, which is shown in Table 5. The contact forces are measured by a calibrated piezo-sensor. The dimensionless parameters are the same as found in literature, namely $\psi = 2.84$ and $\varepsilon = 13$[39]. For information regarding the horizontal granular chain, one can refer to the relevant literature [94]. Furthermore, since the larger initial impact velocity inevitably causes more energy to be dissipated, the CoR in the elastic phase is equal to 0.89. When the elastoplastic contact is activated, the CoR is assumed as 0.70.

In the horizontal granular chain, the critical elastic deformation is equal to 5.4822E-7 m, and the maximum contact deformation between the particles is equal to 7.6394E-6 m. The elastoplastic contact behavior dominates the entire contact process in this granular chain. In Fig. 16, the solitary wave obtained using the new contact model is almost the same as the results using the model used in EDEM software. More importantly, the propagation of solitary waves obtained from the numerical solution is consistent with the experimental data.

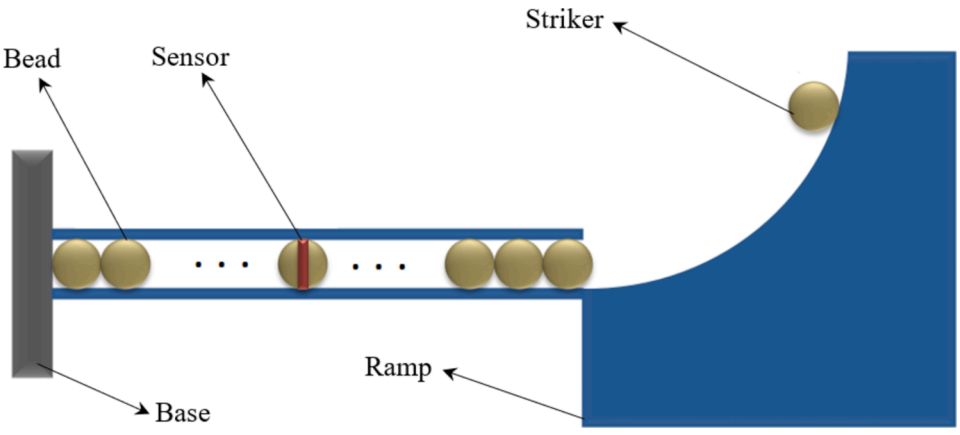

Fig. 15. The experimental setup of the one-dimension granular chain [94].

Table 5
Simulation parameters.

Parameters	Value
Time step	0.01 μs
Simulation time	600 μs
Integrator	Predictor-Corrector (Euler-Trapezoidal)
Radius	2.38 mm
Poisson ratio	0.3
Young's modulus	193 GPa
Yield stress	940 MPa
Mass	0.45 g
Position of the sensor	9,16,24,31,40,50,56,63

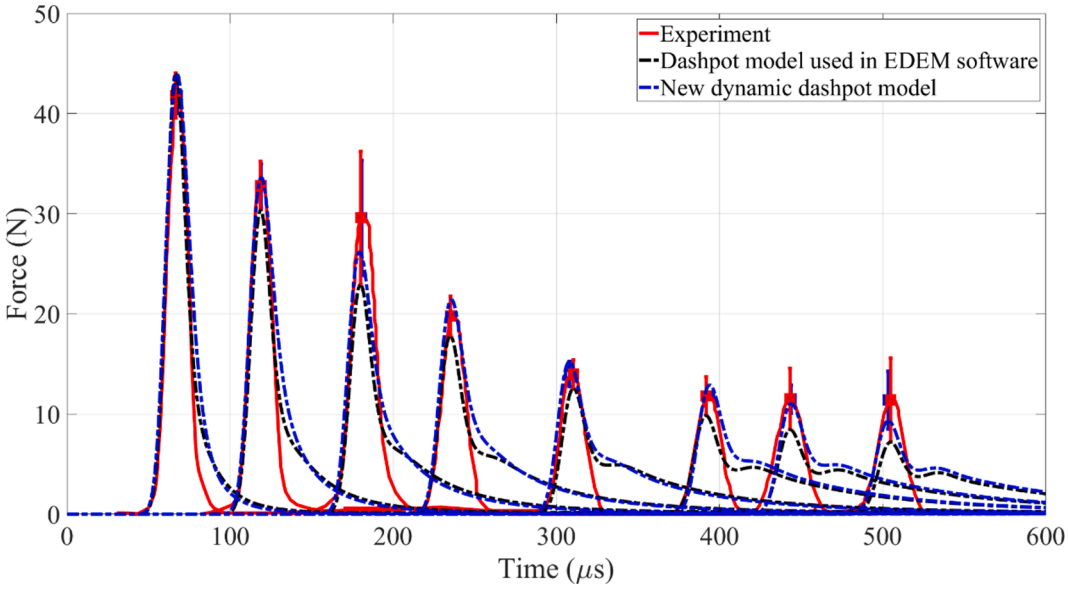

Fig. 16. The solitary wave in the horizontal granular chain.

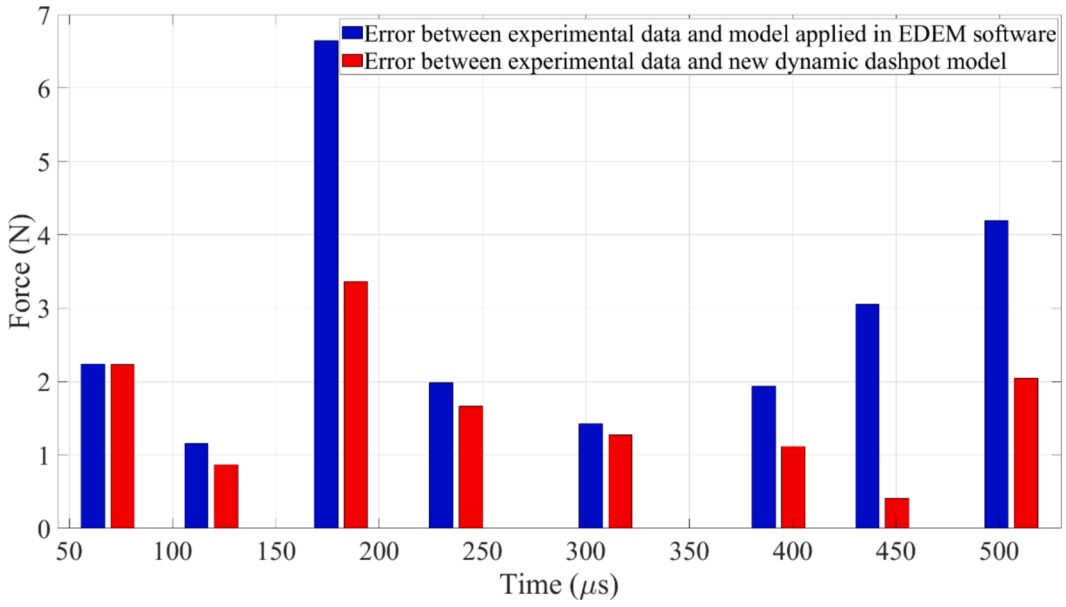

Fig. 17. The error analysis of the peak values in the solitary waves for the horizontal granular chain.

When calculating the peak values in solitary waves, the red error bar between the new contact model and experimental data is smaller than the blue error bar between the model used in EDEM software and experimental data, as shown in Fig. 17. This is mainly because the EDEM contact model utilizes a Hertz contact stiffness to represent the contact stiffness in the elastoplastic phase, which leads to its loss of accuracy compared to the new contact model. Therefore, when the initial impact velocity is small, and the elastic contact behavior dominates the entire contact process, the discrepancy between the new and EDEM contact models can be ignored.

However, when the elastoplastic or plastic contact dominates the entire contact process, the proposed contact model is more accurate than the EDEM contact model because it adopts the ML model to describe the contact stiffness in the elastoplastic or plastic phase rather than the Hertz contact stiffness coefficient. This conclusion indicates that the new contact model possesses a higher accuracy than the model used in the EDEM software when simulating solitary wave propagation in granular systems.

4.3. Hopkinson pressure bar

The Hopkinson pressure bar [36] in Fig. 18 is taken as the other application case to exhibit the properties of this model, which was used to impact a granular chain consisting of 50 identical stainless-steel spheres with a diameter 6.35 mm. The specified structure of this experimental setup can be referred to in this literature [3685]. The material properties of these beads and simulation parameters are displayed in Table 6. The CoR in the elastic phase is equal to 0.81. When the elastoplastic contact is activated, the CoR is assumed as 0.23.

The striker bar velocity is assumed as 13 m/s. In this experimental rig, the elastoplastic phase must be activated under high impact velocity [39]. The contact deformation of the particles can easily reach and beyond the critical elastic deformation 7.4292E-7 m, which inspires the contact phase to come into the elastoplastic contact phase. In Fig. 19, the 40th particle's post-impact velocity is attained by the laser vibrometer, which is the black dash line [36]. It also can be obtained using the proposed contact model, which is almost consistent with the experimental data.

5. Conclusions

The Kelvin-Voigt model inspires this investigation to propose a new contact force model using a frequency-dependent damping factor. However, compared to the Kelvin-Voigt model, the new contact force model avoids the situation where the contact force has a positive value at the beginning of the compression phase, and has a negative value at the end of the recovery phase. This feature is achieved by means of the developed contact model in the elastic phase. Compared to the EDEM contact model, it adopts the ML model to derive the contact stiffness to overcome the deficiency from Hertz contact stiffness in the elastoplastic phase. Compared to the Hunt-Crossley model, it sidesteps the numerical singular issue caused by that the denominator of the damping factor includes the initial impact velocity. Compared to the ML model, it simplifies the calculation strategy of the elastoplastic contact behavior by the viscous damping loop. To summarize, the proposed contact force model can describe a complete contact process that includes elastic, elastoplastic, and plastic phases in sequence. Nevertheless, it still suffers from the occurrence of the tensile force area in the viscous damping loop [54,55], which is mainly caused by the damping force. Further, the capacity of the proposed contact force model describing the energy loss during impact is proved based on the post-impact velocity and Newtonian's CoR definition.

Further, as illustrated, the tensile force area in the viscous damping loop of the new contact force model has no effect on the solitary wave propagation in the granular system, which has been validated by the vertical and horizontal granular chains and Hopkinson pressure bar. That is mainly caused by the multiple compression and multiple impact scenarios in the granular system, which prevents that the contact force comes into the tensile force area in the recovery phase during contact. This study is the first to illustrate why the tensile force does not affect the solitary wave propagation in the granular chain. Moreover, compared to the EDEM contact model, the new contact force model exhibits a significantly higher accuracy when compared to the model applied in EDEM software in the case where the impact event happens under a high impact velocity in the granular system. This is explained by the design of the contact force model, namely that the new contact force model abandons using the Hertz contact stiffness to represent the contact stiffness when the contact behavior comes into the elastoplastic or plastic phase.

While ignoring the plastic flow during impact, the application domain of the proposed contact force model can be summarized as follows: (*i*) it is capable of implementing the common contact behavior between the contact bodies, like the existing contact force

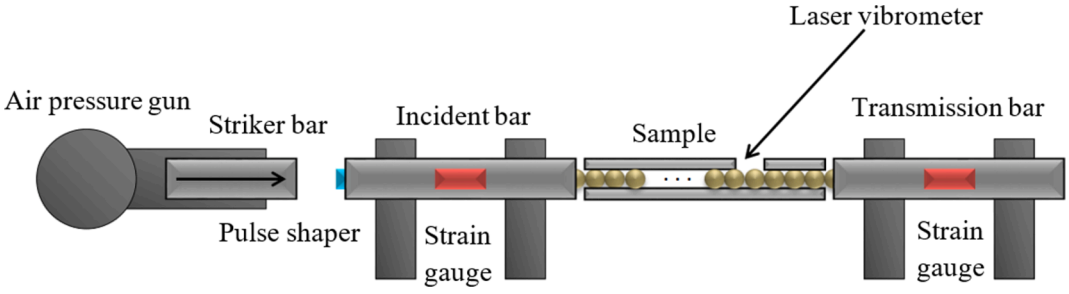

Fig. 18. The experimental setup of the Hopkinson incident bar [36].

Table 6
Simulation parameters.

Parameters	Value
Young's modulus	200 GPa
Poisson ratio	0.307
Yield strength	940 MPa
Contact parameter ε	19
Contact parameter ψ	3.0

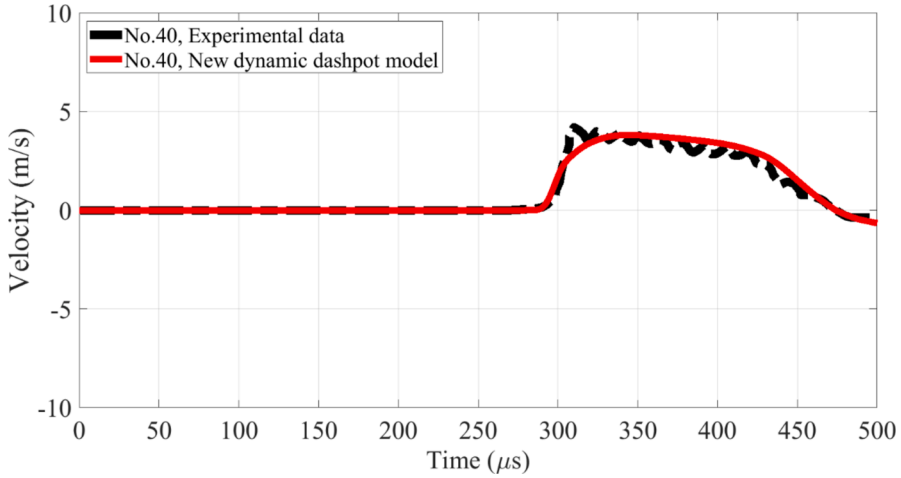

Fig. 19. Post-impact velocity of NO.40 particle.

models with hysteresis damping factors [13,46]; (*ii*) it can be used to calculate the elastoplastic impact behavior, and is capable of describing the whole contact process including the elastic, elastoplastic and plastic phases; (*iii*) it is independent of the initial impact velocity of the contact body, which is suited for the impact behavior of the particles in the granular system; (*iv*) since it employs a damping loop to represent the energy dissipation during impact, which makes it suitable for cases involving multiple compression and impacts between the contact bodies, as occurs in multibody systems (e.g., mechanisms with joint clearance).

CRediT authorship contribution statement

Gengxiang Wang: Writing – original draft, Supervision, Project administration, Methodology, Investigation, Funding acquisition, Conceptualization. **Matthias G.R. Faes:** Writing – original draft. **Tengfei Shi:** Methodology. **Fuan Cheng:** Supervision, Conceptualization. **Yongjun Pan:** Writing – review & editing, Visualization.

Funding

This work is supported by the National Natural Science Foundation of China (Grant NO.12172004).

Declaration of competing interest

The authors declare that they have no known competing financial interests or personal relationships that could have appeared to influence the work reported in this paper.

Data availability

Data will be made available on request.

References

[1] S. Sen, J. Hong, J. Bang, E. Avalos, R. Doney, Solitary waves in the granular chain, Phys. Rep. 462 (2008) 21–66, https://doi.org/10.1016/j.physrep.2007.10.007.
[2] A. Rosas, K. Lindenberg, Pulse propagation in granular chains, Phys. Rep. 735 (2018) 1–37, https://doi.org/10.1016/j.physrep.2018.02.001.
[3] S. Karimnejad, A.A. Delouei, H. Başağaoğlu, M. Nazari, M. Shahmardan, G. Falcucci, M. Lauricella, S. Succi, A Review on Contact and Collision Methods for Multi-Body Hydrodynamic Problems in Complex Flows, Commun, Comput. Phys. 32 (2022) 899–950, https://doi.org/10.4208/cicp.RE-2022-0041.

[4] C. Min, Y. Pan, W. Dai, I. Kawsar, Z. Li, G. Wang, Trajectory optimization of an electric vehicle with minimum energy consumption using inverse dynamics model and servo constraints, Mech. Mach. Theory 181 (2023) 105185, https://doi.org/10.1016/j.mechmachtheory.2022.105185.
[5] Z. Zhao, C. Liu, B. Brogliato, Energy dissipation and dispersion effects in granular media, Phys. Rev. E - Stat. Nonlinear, Soft Matter Phys. 78 (2008) 1–13, https://doi.org/10.1103/PhysRevE.78.031307.
[6] W. Kang, Y. Feng, C. Liu, R. Blumenfeld, Archimedes' law explains penetration of solids into granular media, Nat. Commun. 9 (2018) 1–9, https://doi.org/10.1038/s41467-018-03344-3.
[7] Y. Feng, S. Huang, Y. Pang, K. Huang, C. Liu, Granular dynamics in auger sampling, J. Fluid Mech. 935 (2022) 1–22, https://doi.org/10.1017/jfm.2022.17.
[8] W. Zhang, J. Xu, Toward understanding solitary wave propagation in composite-cylinders-based 1D granular crystals, Extrem. Mech. Lett. 43 (2021) 101156, https://doi.org/10.1016/j.eml.2020.101156.
[9] A. Rosas, A.H. Romero, V.F. Nesterenko, K. Lindenberg, Observation of two-wave structure in strongly nonlinear dissipative granular chains, PhysRevLett. 98 (2007) 98–101, https://doi.org/10.1103/PhysRevLett.98.164301.
[10] M.S.H. Al-Furjan, M.X. Xu, A. Farrokhian, G.S. Jafari, X. Shen, R. Kolahchi, On wave propagation in piezoelectric-auxetic honeycomb-2D-FGM micro-sandwich beams based on modified couple stress and refined zigzag theories, Waves Random Complex Media (2022), https://doi.org/10.1080/17455030.2022.2030499.
[11] F. Santibanez, R. Munoz, A. Caussarieu, S. Job, F. Melo, Experimental evidence of solitary wave interaction in Hertzian chains, Phys. Rev. E - Stat. Nonlinear, Soft Matter Phys. 84 (2011) 1–5, https://doi.org/10.1103/PhysRevE.84.026604.
[12] M.R. Brake, An analytical elastic-perfectly plastic contact model, Int. J. Solids Struct. 49 (2012) 3129–3141, https://doi.org/10.1016/j.ijsolstr.2012.06.013.
[13] M. Rodrigues da Silva, F. Marques, M. Tavares da Silva, P. Flores, A compendium of contact force models inspired by Hunt and Crossley's cornerstone work, Mech. Mach. Theory 167 (2022) 104501, https://doi.org/10.1016/j.mechmachtheory.2021.104501.
[14] R. Gunes, M. Aydin, M.K. Apalak, J.N. Reddy, The elasto-plastic impact analysis of functionally graded circular plates under low-velocities, Compos. Struct. 93 (2011) 860–869, https://doi.org/10.1016/j.compstruct.2010.07.008.
[15] W.J. Stronge, A.R. Sofi, B. Ravani, Computing the composite coefficient of restitution for inelastic impact of dissimilar bodies, Int. J. Impact Eng. 133 (2019) 1–11, https://doi.org/10.1016/j.ijimpeng.2019.103333.
[16] E. Olsson, P.L. Larsson, A unified model for the contact behaviour between equal and dissimilar elastic-plastic spherical bodies, Int. J. Solids Struct. 81 (2016) 23–32, https://doi.org/10.1016/j.ijsolstr.2015.10.004.
[17] R.L. Jackson, I. Green, D.B. Marghitu, Predicting the coefficient of restitution of impacting elastic-perfectly plastic spheres, Nonlinear Dyn. 60 (2010) 217–229, https://doi.org/10.1007/s11071-009-9591-z.
[18] W.R. Chang, F.F. Ling, Normal impact model of rough surfaces, J. Tribol. 114 (1992) 439–447, https://doi.org/10.1115/1.2920903.
[19] B. Bhushan, Contact mechanics of rough surfaces in tribology: Multiple asperity contact, Tribol. Lett. 4 (1998) 1–35, https://doi.org/10.1023/A:1019186601445.
[20] D. Tabor, A Simple Theory of Static and Dynamic Hardness, Proc. r. Soc. London. Ser. a. Math. Phys. Sci. 192 (1948) 247–274.
[21] C.H. Lee, S. Masaki, S. Kobayashi, Analysis of ball indentation, Int. J. Mech. Sci. 14 (1972) 417–426, https://doi.org/10.1016/0020-7403(72)90099-9.
[22] G.B. Sinclair, P.S. Follansbee, K.J. Johnson, Quasi-static normal indentation of an elasto-plastic half-space by a rigid circular cylinder of infinite length, Int. J. Solids Struct. 22 (1986) 919–934, https://doi.org/10.1016/0020-7683(86)90071-5.
[23] E. Corral, M.J.G. García, C. Castejon, J. Meneses, R. Gismeros, Dynamic modeling of the dissipative contact and friction forces of a passive biped-walking robot, Appl. Sci. 10 (2020), https://doi.org/10.3390/app10072342.
[24] R. Gismeros Moreno, E. Corral Abad, J. Meneses Alonso, M.J. Gómez García, C., Castejón Sisamón, Modelling multiple-simultaneous impact problems with a nonlinear smooth approach: pool/billiard application, Nonlinear Dyn. 107 (2022) 1859–1886, https://doi.org/10.1007/s11071-021-07117-4.
[25] M.R. Brake, P.L. Reu, D.J. VanGoethem, M.V. Bejarano, A. Sumali, Experimental validation of an elastic-plastic contact model, ASME 2011 Int, Mech. Eng. Congr. Expo. IMECE 2011 (7) (2011) 733–744, https://doi.org/10.1115/imece2011-65736.
[26] W.R. Chang, I. Etsion, D.B. Bogy, An elastic-plastic model for the contact of rough surfaces, J. Tribol. 109 (1987) 257–263, https://doi.org/10.1115/1.3261348.
[27] K.L. Johnson, L.M. Keer, Contact Mechanics (1986), https://doi.org/10.1115/1.3261297.
[28] W.J. Stronge, Contact Problems for Elasto-Plastic Impact in Multi-Body Systems, in: Impacts Mech. Syst., 2000: pp. 189–234. https://doi.org/10.1007/3-540-45501-9_4.
[29] R.L. Jackson, I. Green, A finite element study of elasto-plastic hemispherical contact against a rigid flat, J. Tribol. 127 (2005) 343–354, https://doi.org/10.1115/1.1866166.
[30] L. Kogut, I. Etsion, Elastic-plastic contact analysis of a sphere and a rigid flat, J. Appl. Mech. 69 (2002) 657–662, https://doi.org/10.1115/1.1490373.
[31] S. Shankar, M.M. Mayuram, A finite element based study on the elastic-plastic transition behavior in a hemisphere in contact with a rigid flat, J. Tribol. 130 (2008) 1–6, https://doi.org/10.1115/1.2958081.
[32] L. Vu-Quoc, X. Zhang, L. Laesburg, A normal force-Displacement model for contacting spheres accounting for plastic deformation: Force-Driven formulation, J. Appl. Mech. Trans. ASME 67 (2000) 363–371, https://doi.org/10.1115/1.1305334.
[33] L. Vu-Quoc, X. Zhang, L. Lesburg, Normal and tangential force-displacement relations for frictional elasto-plastic contact of spheres, Int. J. Solids Struct. 38 (2001) 6455–6489, https://doi.org/10.1016/S0020-7683(01)00065-8.
[34] Y. Du, S. Wang, Energy dissipation in normal elastoplastic impact between two spheres, J. Appl. Mech. Trans. ASME 76 (2009) 1–8, https://doi.org/10.1115/1.3130801.
[35] N. Ye, K. Komvopoulos, Indentation analysis of elastic-plastic homogeneous and layered media: Criteria for determining the real material hardness, J. Tribol. 125 (2003) 685–691, https://doi.org/10.1115/1.1572515.
[36] H.A. Burgoyne, C. Daraio, Elastic-plastic wave propagation in uniform and periodic granular chains, J. Appl. Mech. Trans. ASME 82 (2015) 1–10, https://doi.org/10.1115/1.4030458.
[37] H.A. Burgoyne, C. Daraio, Strain-rate-dependent model for the dynamic compression of elastoplastic spheres, Phys. Rev. E - Stat. Nonlinear, Soft Matter Phys. 89 (2014) 1–5, https://doi.org/10.1103/PhysRevE.89.032203.
[38] D. Ma, C. Liu, Contact Law and Coefficient of Restitution in Elastoplastic Spheres, J. Appl. Mech. 82 (2015) 1–9, https://doi.org/10.1115/1.4031483.
[39] Y. Feng, W. Kang, D. Ma, C. Liu, Multiple Impacts and Multiple-Compression Process in the Dynamics of Granular Chains, J. Comput. Nonlinear Dyn. 14 (2019), https://doi.org/10.1115/1.4044584.
[40] M. Shoaib, L. Kari, Discrete element simulation of elastoplastic shock wave propagation in spherical particles, Adv. Acoust. Vib. 2011 (2011), https://doi.org/10.1155/2011/123695.
[41] E. Wang, M. Manjunath, A.P. Awasthi, R.K. Pal, P.H. Geubelle, J. Lambros, High-amplitude elastic solitary wave propagation in 1-D granular chains with preconditioned beads: Experiments and theoretical analysis, J. Mech. Phys. Solids 72 (2014) 161–173, https://doi.org/10.1016/j.jmps.2014.08.002.
[42] R.K. Pal, A.P. Awasthi, P.H. Geubelle, Wave propagation in elasto-plastic granular systems, Granul. Matter 15 (2013) 747–758, https://doi.org/10.1007/s10035-013-0449-1.
[43] H.M. Lankaranl, P.E. Nlkravesh, A contact force model with hysteresis damping for impact analysis of mul tl body systems, Proc. ASME Des. Eng. Tech. Conf. 3 (1989) 45–51, https://doi.org/10.1115/DETC1989-0117.
[44] H.B. Amnieh, M.S. Zamzam, R. Kolahchi, Dynamic analysis of non-homogeneous concrete blocks mixed by SiO2 nanoparticles subjected to blast load experimentally and theoretically, Constr. Build. Mater. 174 (2018) 633–644, https://doi.org/10.1016/j.conbuildmat.2018.04.140.
[45] Y. Tsuji, T. Tanaka, T. Ishida, Lagrangian numerical simulation of plug flow of cohesionless particles in a horizontal pipe, Powder Technol. 71 (1992) 239–250, https://doi.org/10.1016/0032-5910(92)88030-L.
[46] F. Marques, I. Roupa, M.T. Silva, P. Flores, H.M. Lankarani, Examination and comparison of different methods to model closed loop kinematic chains using Lagrangian formulation with cut joint, clearance joint constraint and elastic joint approaches, Mech. Mach. Theory 160 (2021) 104294, https://doi.org/10.1016/j.mechmachtheory.2021.104294.

[47] M.S.H. Al-Furjan, C. Yin, X. Shen, R. Kolahchi, M.S. Zarei, M.H. Hajmohammad, Energy absorption and vibration of smart auxetic FG porous curved conical panels resting on the frictional viscoelastic torsional substrate, Mech. Syst. Signal Process. 178 (2022) 109269, https://doi.org/10.1016/j.ymssp.2022.109269.
[48] M. Machado, P. Moreira, P. Flores, H.M. Lankarani, Compliant contact force models in multibody dynamics: Evolution of the Hertz contact theory, Mech. Mach. Theory 53 (2012) 99–121, https://doi.org/10.1016/j.mechmachtheory.2012.02.010.
[49] J. Zhang, X. Liang, Z. Zhang, G. Feng, Q. Zhao, L. Zhao, G. He, A continuous contact force model for impact analysis, Mech. Syst. Signal Process. 168 (2022) 108739, https://doi.org/10.1016/j.ymssp.2021.108739.
[50] G. Wang, C. Liu, Y. Liu, Energy Dissipation Analysis for Elastoplastic Contact and Dynamic Dashpot Models, Int. J. Mech. Sci. 221 (2022) 107214, https://doi.org/10.1016/j.ijmecsci.2022.107214.
[51] J. Ma, G. Chen, L. Ji, L. Qian, S. Dong, A general methodology to establish the contact force model for complex contacting surfaces, Mech. Syst. Signal Process. 140 (2020) 106678, https://doi.org/10.1016/j.ymssp.2020.106678.
[52] P. Zhao, J. Liu, Y. Li, C. Wu, A spring-damping contact force model considering normal friction for impact analysis, Nonlinear Dyn. 105 (2021) 1437–1457, https://doi.org/10.1007/s11071-021-06660-4.
[53] P. Flores, Contact mechanics for dynamical systems: a comprehensive review, Multibody Syst. Dyn. 54 (2022) 127–177, https://doi.org/10.1007/s11044-021-09803-y.
[54] C. Spitas, M.S. Dwaikat, V. Spitas, Effect of the elastic hysteresis term formulation and response to non-harmonic periodic excitations of a non-linear SDOF dynamical model with weak frequency-dependency in the time domain, Proc. Inst. Mech. Eng. Part C J. Mech. Eng. Sci. 235 (2021) 4637–4647, https://doi.org/10.1177/09544062211018252.
[55] M.M.S. Dwaikat, C. Spitas, V. Spitas, A non-linear model for elastic hysteresis in the time domain: Implementation for multiple degrees of freedom, Proc. Inst. Mech. Eng. Part C J. Mech. Eng. Sci. 235 (2021) 4612–4624.
[56] K.H. Hunt, F.R.E. Crossley, E. Crossley, Coefficient of restitution interpreted as damping in vibroimpact, J. Appl. Mech. 42 (1975) 440–445, https://doi.org/10.1115/1.3423596.
[57] J. Lee, H.J. Herrmann, Angle of repose and angle of marginal stability: Molecular dynamics of granular particles, J. Phys. a. Math. Gen. 26 (1993) 373–383, https://doi.org/10.1088/0305-4470/26/2/021.
[58] T.W. Lee, A.C. Wang, On the dynamics of intermittent-motion mechanisms. Part 1: dynamic model and response, J. Mech. Transm. Autom. Des. 105 (1983) 534–540.
[59] G. Hu, Z. Hu, B. Jian, L. Liu, H. Wan, On the determination of the damping coefficient of non-linear spring-dashpot system to model hertz contact for simulation by discrete element method, J. Comput. 6 (2011) 984–988, https://doi.org/10.4304/jcp.6.5.984-988.
[60] H.M. Lankarani, P.E. Nikravesh, A contact force model with hysteresis damping for impact analysis of multibody systems, J. Mech. Des. Trans. ASME 112 (1990) 369–376, https://doi.org/10.1115/1.2912617.
[61] P. Flores, M. MacHado, M.T. Silva, J.M. Martins, On the continuous contact force models for soft materials in multibody dynamics, Multibody Syst. Dyn. 25 (2011) 357–375, https://doi.org/10.1007/s11044-010-9237-4.
[62] H.M. Lankarani, P.E. Nikravesh, Continuous contact force models for impact analysis in multibody systems, Nonlinear Dyn. 5 (1994) 193–207, https://doi.org/10.1007/BF00045676.
[63] Y. Gonthier, J. Mcphee, C. Lange, J.C. Piedbœuf, A regularized contact model with asymmetric damping and dwell-time dependent friction, Multibody Syst. Dyn. 11 (2004) 209–233, https://doi.org/10.1023/B:MUBO.0000029392.21648.bc.
[64] S. Hu, X. Guo, A dissipative contact force model for impact analysis in multibody dynamics, Multibody Syst. Dyn. 35 (2015) 131–151, https://doi.org/10.1007/s11044-015-9453-z.
[65] C. Spitas, M.M.S. Dwaikat, V. Spitas, Non-linear modelling of elastic hysteretic damping in the time domain, Arch. Mech. 72 (2020) 323–353. https://doi.org/10.24423/aom.3536.
[66] J. Alves, N. Peixinho, M.T. Da Silva, P. Flores, H.M. Lankarani, A comparative study of the viscoelastic constitutive models for frictionless contact interfaces in solids, Mech. Mach. Theory 85 (2015) 172–188, https://doi.org/10.1016/j.mechmachtheory.2014.11.020.
[67] B. Brogliato, Nonsmooth Mechanics: Models, Springer B, Springer International Publishing Switzerland, Dynamics and Control, 2016.
[68] J.J. Lou, C.B. Li, An improved model of contact collision investigation on multi-body systems with revolute clearance joints, Proc. Inst. Mech. Eng. Part D J. Automob. Eng. 234 (2020) 2103–2112, https://doi.org/10.1177/0954407019868124.
[69] J. Ma, S. Dong, G. Chen, P. Peng, L. Qian, A data-driven normal contact force model based on artificial neural network for complex contacting surfaces, Mech. Syst. Signal Process. 156 (2021) 107612, https://doi.org/10.1016/j.ymssp.2021.107612.
[70] J. Zhang, W. Li, L. Zhao, G. He, A continuous contact force model for impact analysis in multibody dynamics, Mech. Mach. Theory 153 (2020) 103946, https://doi.org/10.1016/j.mechmachtheory.2020.103946.
[71] H. Safaeifar, A. Farshidianfar, A new model of the contact force for the collision between two solid bodies, Multibody Syst. Dyn. 50 (2020) 233–257, https://doi.org/10.1007/s11044-020-09732-2.
[72] M. Poursina, P.E. Nikravesh, Optimal damping coefficient for a class of continuous contact models, Multibody Syst. Dyn. 50 (2020) 169–188, https://doi.org/10.1007/s11044-020-09745-x.
[73] G. Kuwabara, K. Kono, Restitution coefficient in a collision between two spheres, Jpn. J. Appl. Phys. 26 (1987) 1230–1233, https://doi.org/10.1143/JJAP.26.1230.
[74] R. Jankowski, Analytical expression between the impact damping ratio and the coefficient of restitution in the non-linear viscoelastic model of structural pounding, Earthq. Eng. Struct. Dyn. 35 (2006) 517–524, https://doi.org/10.1002/eqe.537.
[75] R. Jankowski, Non-linear viscoelastic modelling of earthquake-induced structural pounding, Earthq. Eng. Struct. Dyn. 34 (2005) 595–611, https://doi.org/10.1002/eqe.434.
[76] T. Schwager, T. Pöschel, Coefficient of normal restitution of viscous particles and cooling rate of granular gases, Phys. Rev. E - Stat. Physics, Plasmas, Fluids, Relat. Interdiscip. Top. 57 (1998) 650–654, https://doi.org/10.1103/PhysRevE.57.650.
[77] G. Ristow, Simulating granular flow with molecular dynamics, J. Phys. I (2) (1992) 649–662.
[78] F. Isaac, F. Marques, N. Dourado, P. Flores, A finite element model of a 3D dry revolute joint incorporated in a multibody dynamic analysis, Multibody Syst. Dyn. 45 (2019) 293–313, https://doi.org/10.1007/s11044-018-09659-9.
[79] M. Gabiccini, F. Fusco, On state and inertial parameter estimation of free-falling planar rigid bodies subject to unscheduled frictional impacts, Mech. Mach. Theory 141 (2019) 171–195, https://doi.org/10.1016/j.mechmachtheory.2019.07.010.
[80] M.S.H. Al-Furjan, M.H. Hajmohammad, X. Shen, D.K. Rajak, R. Kolahchi, Evaluation of tensile strength and elastic modulus of 7075-T6 aluminum alloy by adding SiC reinforcing particles using vortex casting method, J. Alloys Compd. 886 (2021) 161261, https://doi.org/10.1016/j.jallcom.2021.161261.
[81] P. Flores, J. Ambrósio, H.M. Lankarani, Contact-impact events with friction in multibody dynamics: Back to basics, Mech. Mach. Theory 184 (2023), https://doi.org/10.1016/j.mechmachtheory.2023.105305.
[82] M. Wojtkowski, J. Pecen, J. Horabik, M. Molenda, Rapeseed impact against a flat surface: Physical testing and DEM simulation with two contact models, Powder Technol. 198 (2010) 61–68, https://doi.org/10.1016/j.powtec.2009.10.015.
[83] Y. Pan, Y. Sun, Z. Li, P. Gardoni, Machine learning approaches to estimate suspension parameters for performance degradation assessment using accurate dynamic simulations, Reliab. Eng. Syst. Saf. 230 (2023) 108950, https://doi.org/10.1016/j.ress.2022.108950.
[84] G. Wang, C. Liu, Nonlinear wave in granular systems based on elastoplastic dashpot model, Int. J. Mech. Syst. Dyn. 1 (2021) 132–142, https://doi.org/10.1002/msd2.12008.
[85] G. Wang, D. Ma, C. Liu, Y. Liu, Development of a compliant dashpot model with nonlinear and linear behaviors for the contact of multibody systems, Mech. Syst. Signal Process. 185 (2023) 109785, https://doi.org/10.1016/j.ymssp.2022.109785.
[86] G. Wang, M.G.R. Faes, F. Cheng, T. Shi, P. Gao, Extension of dashpot model with elastoplastic deformation and rough surface in impact behavior, Chaos Solitons Fractals 162 (2022) 112402, https://doi.org/10.1016/j.chaos.2022.112402.

[87] M. Bar-Hen, I. Etsion, Experimental study of the effect of coating thickness and substrate roughness on tool wear during turning, Tribol. Int. 110 (2017) 341–347, https://doi.org/10.1016/j.triboint.2016.11.011.
[88] A. Pazouki, M. Kwarta, K. Williams, W. Likos, R. Serban, P. Jayakumar, D. Negrut, Compliant contact versus rigid contact: A comparison in the context of granular dynamics, PhysRevE 96 (2017) 1–13, https://doi.org/10.1103/PhysRevE.96.042905.
[89] L. Fang, R. Zhang, C. Vanden Heuvel, R. Serban, D. Negrut, Chrono::GPU: An open-source simulation package for granular dynamics using the discrete element method, Processes 9 (2021), https://doi.org/10.3390/pr9101813.
[90] M. Rakhsha, C. Kelly, N. Olsen, R. Serban, D. Negrut, Multibody dynamics versus fluid dynamics: Two perspectives on the dynamics of granular flows, J. Comput. Nonlinear Dyn. 15 (2020) 1–10, https://doi.org/10.1115/1.4047237.
[91] T. Schwager, T. Pöschel, Coefficient of restitution for viscoelastic spheres: The effect of delayed recovery, Phys. Rev. E - Stat. Nonlinear, Soft Matter Phys. 78 (2008) 1–11, https://doi.org/10.1103/PhysRevE.78.051304.
[92] C. Daraio, V.F. Nesterenko, E.B. Herbold, S. Jin, Energy trapping and shock disintegration in a composite granular medium, PhysRevLett. 96 (2006) 1–4, https://doi.org/10.1103/PhysRevLett.96.058002.
[93] C. Daraio, V.F. Nesterenko, E.B. Herbold, S. Jin, Tunability of solitary wave properties in one-dimensional strongly nonlinear phononic crystals, Phys. Rev. E - Stat. Nonlinear, Soft Matter Phys. 73 (2006) 1–10, https://doi.org/10.1103/PhysRevE.73.026610.
[94] R. Carretero-González, D. Khatri, M.A. Porter, P.G. Kevrekidis, C. Daraio, Dissipative solitary waves in granular crystals, PhysRevLett. 102 (2009) 1–4, https://doi.org/10.1103/PhysRevLett.102.024102.